

# **Chapter 3**

## **RESULTS AND DISCUSSION**

### 3.1. LYSOZYME AND ITS INTERACTIONS WITH [60]FULLERENE

The reaction between [60]fullerene and lysozyme was carried out for 24h in the presence of light. Physical observation revealed that as the time progressed the colour of the reaction mixture changes from violet to brown and subsequently to dark brown leaving some residue in the reaction mixture after completion of 24h. It was then thought to study the effect of time on the reaction. Thus the reaction time was increased to six days. It was observed that after six days, very small amount of the residue remained in the reaction mixture. This observation implies that the encapsulation of [60]fullerene into the lysozyme was slow and required more time to get encapsulated.

The effect of presence and absence of light on reactivity of [60]fullerene was studied. For that same reaction was carried out in the absence of light. No colour change in the reaction mixture was observed after completion of 24h thus the reaction was continued for 6 days but again no physical change in the reaction mixture was observed. From this observation it was considered that there was not any interaction between [60]fullerene and lysozyme in the absence of light.

To study the interaction between [60]fullerene and lysozyme it was presumed that [60]fullerene either reacts with the terminal amino groups or occupies sites within the hydrophobic core of the lysozyme. The interaction between these two molecules was studied using a mixed solvent system that solubilized both lysozyme and the [60]fullerene. Thus an adduct was formed between these two which was easily isolated. This adduct was found to be water-soluble giving an amber colored clear solution. This solution was used for further analysis using Fluorescence, Ultraviolet and FT-IR spectroscopy.

Fluorescence energy transfer study is a versatile technique to study the interactions between any two molecules, provided the emission wavelength of the first molecule overlaps with the excitation wavelength of the second. If the distance between these two molecules is within a certain range ( $50\text{\AA}$ ), then the emission peak of the first molecule either disappears or shows a decreased intensity with the appearance of the emission peak of the second molecule.

The fluorescence spectrum of lysozyme (dissolved in water) was measured at variable light wavelength and is shown in Figure 3.1(a). The aromatic amino acid residues of lysozyme excited at 280nm showed a peak between 300 to 400 nm corresponding to the emission of aromatic residues.

The fluorescence spectrum of the lysozyme-[60]fullerene adduct (dissolved in water) was also measured at variable light wavelength and is displayed in Figure 3.1(b). Surprisingly, the lysozyme-[60]fullerene adduct did not show the typical emission peak of the lysozyme instead an intense peak was observed between 400 to 450 nm which results from the energy transfer between the excited aromatic residue and the [60]fullerene. This implies that there is an interaction between the two molecules that could be either of the covalent or of noncovalent type.

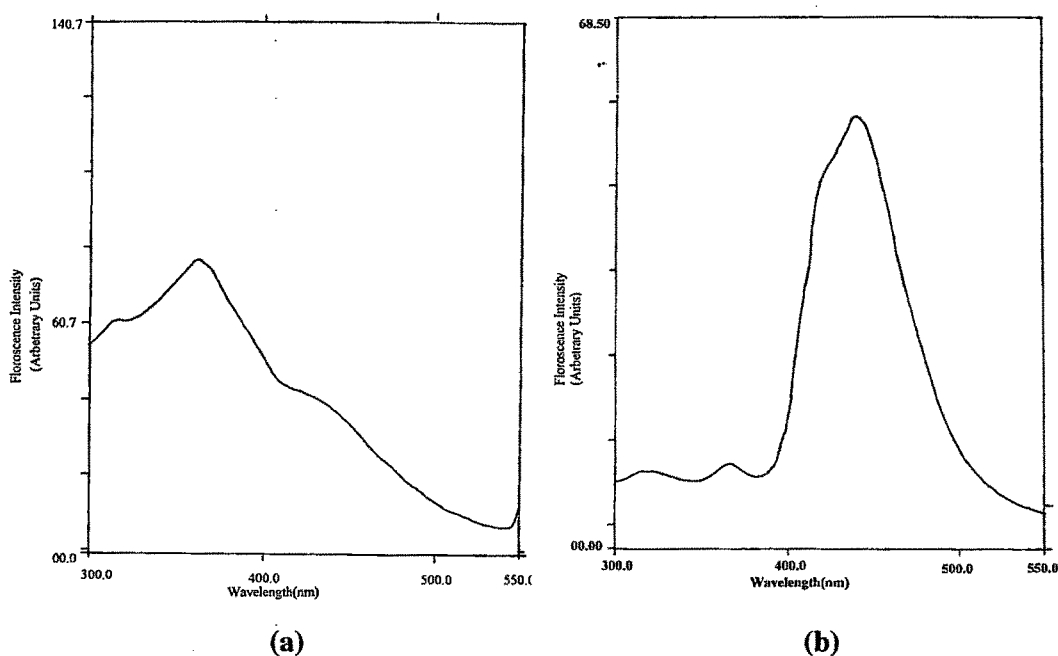
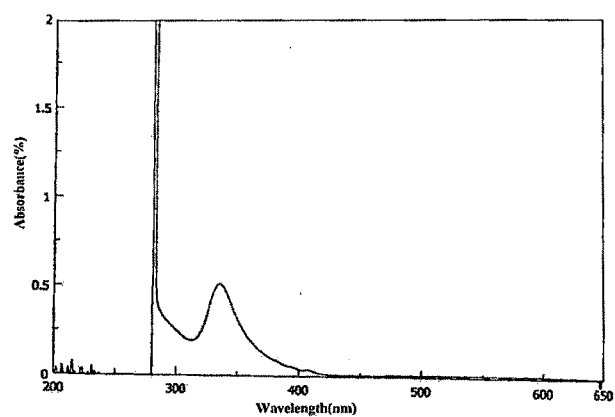


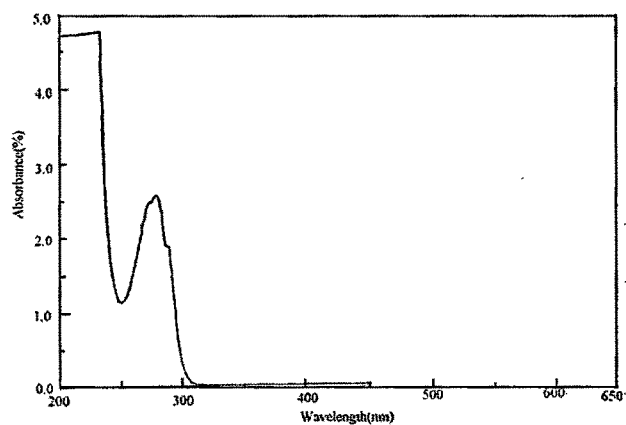
**Figure 3.1.** Fluorescence spectrum of (a) lysozyme and (b) lysozyme-[60]fullerene adduct in water.

The UV-VIS absorbance spectroscopy was used to further confirm the interactions between lysozyme and [60]fullerene. The UV-VIS spectrum of [60]fullerene dissolved in toluene was taken and is shown in Figure 3.2(a). Furthermore, the UV-VIS spectrum of lysozyme as well as lysozyme-[60]fullerene adduct was also taken and is shown in Figure 3.2(b) and Figure 3.2(c), respectively.

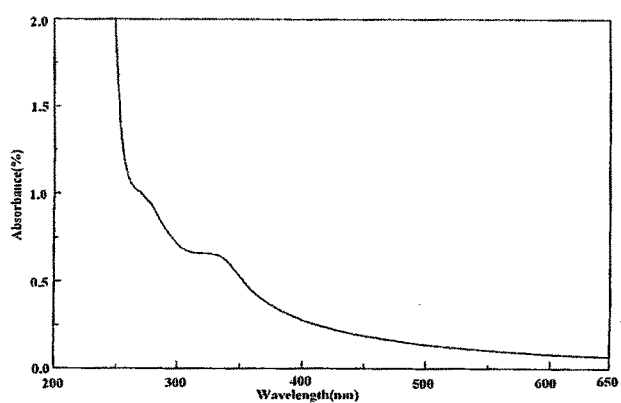
The [60]fullerene showed an absorbance maxima at around 330 nm in toluene [Figure 3.2(a)] and is water-insoluble, whereas lysozyme shows an absorbance maximum at 280 nm in water [Figure 3.2(b)]. The spectra of the adduct in water showed the typical absorbance peak of lysozyme and a small peak corresponding to the [60]fullerene. Both these peaks are red-shifted by a few nanometers [Figure. 3.2(c)], thus confirming the interaction between these two molecules. There is a broadening of the absorbance beyond 400nm typical of the [60]fullerene absorbance in organic solvents.



(a)



(b)



(c)

**Figure 3.2.** UV-Visible spectrum of (a) [60]fullerene in toluene (b) lysozyme in water and (c) [60]fullerene-lysozyme adduct in water.

At this junction it is important to understand the nature of the interaction between [60]fullerene and lysozyme. Lysozyme has free N-terminal amino group and some amino groups present along the side chains of the basic amino acid residues which can form covalent bonds with the [60]fullerene. The fluorescence energy transfer studies and UV-VIS absorbance studies do not give any indication about the nature of the binding between [60]fullerene and lysozyme.

To understand the nature of the interaction between the [60]fullerene and lysozyme an aqueous solution of the adduct was shaken with toluene for few minutes and the UV absorbances of the aqueous phase, given in Figure 3.3(d) and the organic phase, given in Figure 3.2(e) were recorded. The aqueous phase showed the typical absorbance of lysozyme with the disappearance of the absorbance peak corresponding to that of [60]fullerene observed in the aqueous solution of the adduct. This suggests that there is no covalent bond formation between the two and the interaction observed in the fluorescence studies is hydrophobic in nature.

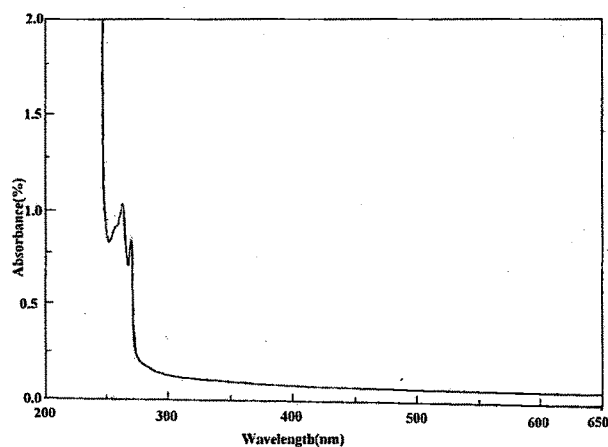


**Figure 3.2(d).** UV-Visible spectrum for [60]fullerene-lysozyme adduct in aqueous layer.

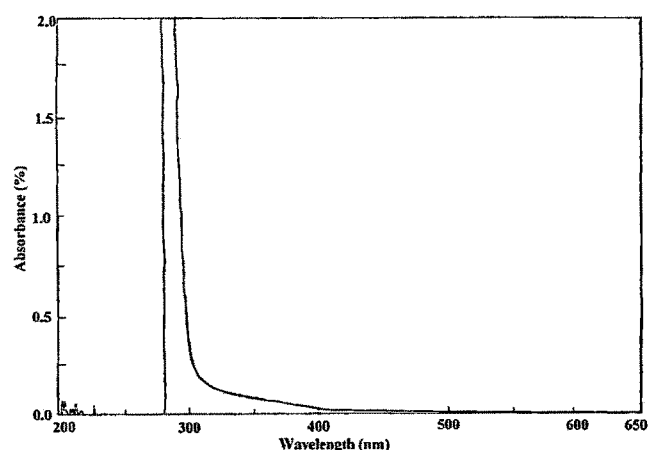


**Figure 3.2(e).** UV-Visible spectrum for [60]fullerene-lysozyme adduct in toluene layer.

FT-IR spectra also confirms the [60]fullerene-lysozyme adduct formation showing the typical peak of [60]fullerene at 1414 and 668  $\text{cm}^{-1}$ .

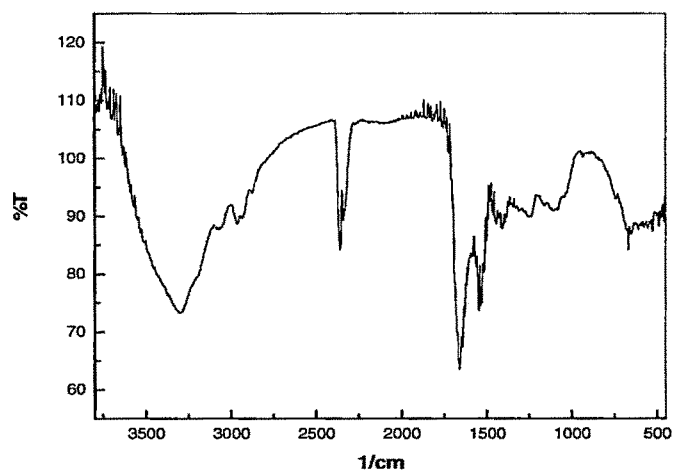


**Figure 3.3.** FT-IR Spectra of [60]fullerene-lysozyme adduct.

This was further confirmed by denaturing polyacrylamide gel electrophoresis where in proteins are boiled in a solution containing sodium dodecyl sulphate (SDS). The SDS being a chaotropic anionic detergent binds the protein backbone in a fixed ratio of one SDS molecule per every two amino acid residues and envelops the original charges

present on the protein. The binding of SDS also causes denaturation of proteins making them into linear rods. When SDS bound proteins are subjected to gel electrophoresis they are resolved into separate bands according to their molecular weights. After carrying out electrophoresis of [60]fullerene–lysozyme adduct with lysozyme as a control, it was observed that the adduct showed a band parallel to lysozyme control, ruling out any change in its molecular weight after binding to fullerene. This lends support to our earlier observation that the interaction between the two molecules is purely hydrophobic, which was disrupted by SDS.



### 3.2 [60]FULLERENE-ITS FORMATION OF REVERSE MICELLE AND MICROEMULSION STUDIES

#### 3.2.1 Critical Reverse Micelle Formation

The technique of determination of reverse micelle concentration (crmc) by the iodine solubilization method is well known. It has been shown that this technique can be applied to both aqueous and nonaqueous solutions. Though [60]fullerene is a highly hydrophobic and nonpolar molecule, it was found to form a reverse micelle complex with Span 60 and Brij 35 in toluene.

The  $\lambda_{\max}$  of pure [60]fullerene( $1.39 \times 10^{-4}$  M) solution was found to be 312nm. However  $\lambda_{\max}$  of [60]fullerene-Span 60 solution was at 323 nm and [60]fullerene-Brij 35 solution was at 326 nm. The fullerene-reverse micelle complex gives rise to this new  $\lambda_{\max}$  that has shown a shift of 11 nm and 14 nm respectively towards the higher wavelength and is shown in the Figure 3.4 and Figure 3.6. As expected the absorbance of the solution with surfactant was lower than that of the pure fullerene solution in both the systems.

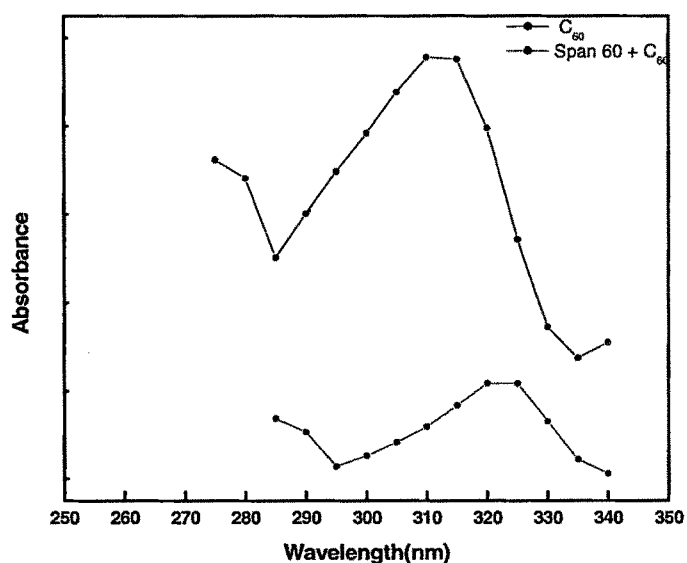


**Figure 3.4.** Plot of absorbance vs. wavelength to determine  $\lambda_{\max}$  of [60]fullerene-Span 60 solution.

The formation of micelle and its variation with the concentration of the surfactant were done at this new wavelength (323nm & 326nm). The absorbance values were plotted against the different concentration of surfactants used and were noted at 30°C & 40°C. It was observed that change in absorbance value with concentration was not linear but showed a distinct break point and is shown in Figure 3.5 and Figure 3.7. These break points were taken as cmc of reverse micellization at corresponding temperatures and these values are shown in Table 3.1 and Table 3.2 for Span 60 and Brij 35 respectively. After break point at particular concentration the absorbance was steep. The slope was sharper at lower temperature than at 40°C.

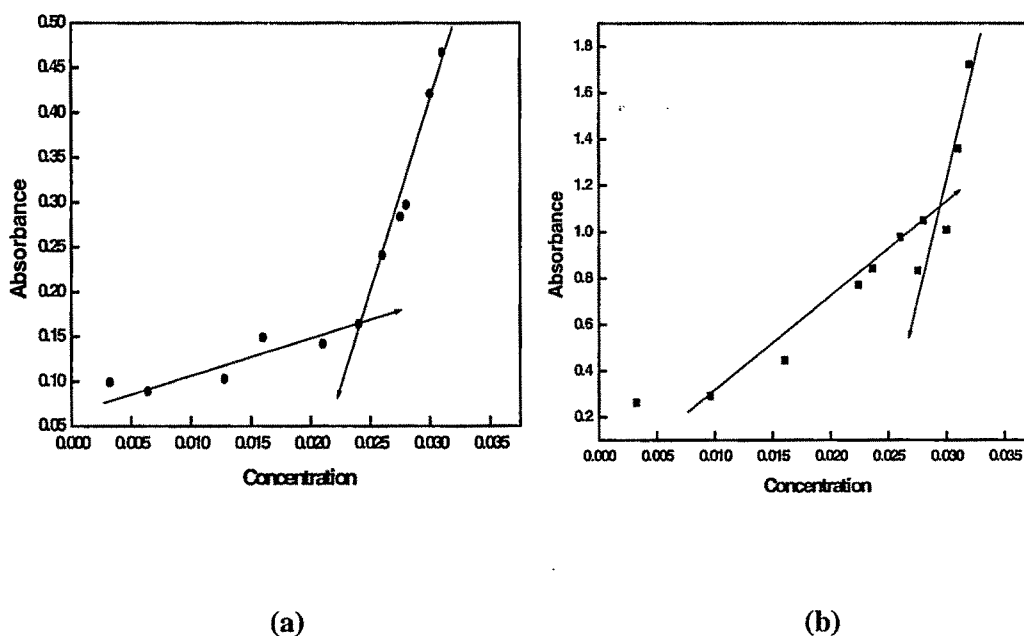


**Figure 3.5.** Plot of absorbance vs. concentration of Span 60 in the presence of [60]fullerene to determine cmc at (a) 30°C and (b) 40°C.

The values of crmc can be calculated at different temperatures. Based on the crmc values the standard free energy; enthalpy and entropy of reverse micellization were calculated by using the well known relations (valid for nonionic surfactants) and are presented in Table 3.1 & Table 3.2.

$$\Delta G_{rm}^{\circ} = RT \ln (crmc)$$

$$\Delta H_{rm}^{\circ} = -RT^2 d \ln (crmc)/dT$$

$$\Delta S_{rm}^{\circ} = (\Delta H_{rm}^{\circ} - \Delta G_{rm}^{\circ}) / T$$

**Table 3.1.** Critical reverse micelle concentration, free energy, enthalpy and entropy of reverse micellization of Span 60 in toluene-[60]fullerene solution at 30°C and 40°C.

Temperature	Crmc	$-\Delta G_{rm}^{\circ}$	$-\Delta H_{rm}^{\circ}$	$-\Delta S_{rm}^{\circ}$
°C	mmol dm <sup>-3</sup>	kJmol <sup>-1</sup>	kJmol <sup>-1</sup>	Jmol <sup>-1</sup> K <sup>-1</sup>
30	0.024	92.66	112.92	0.066
40	0.0284	100.12	126.37	0.076

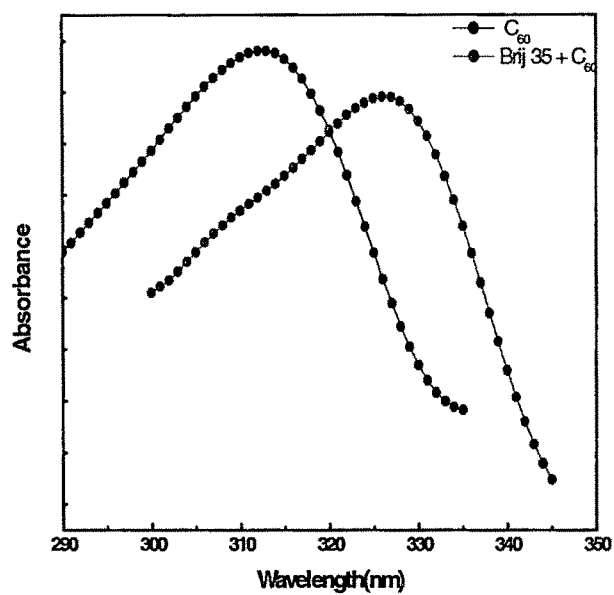


**Figure 3.6.** Plot of absorbance vs. wavelength to determine  $\lambda_{\max}$  of [60]fullerene-Brij 35 solution.

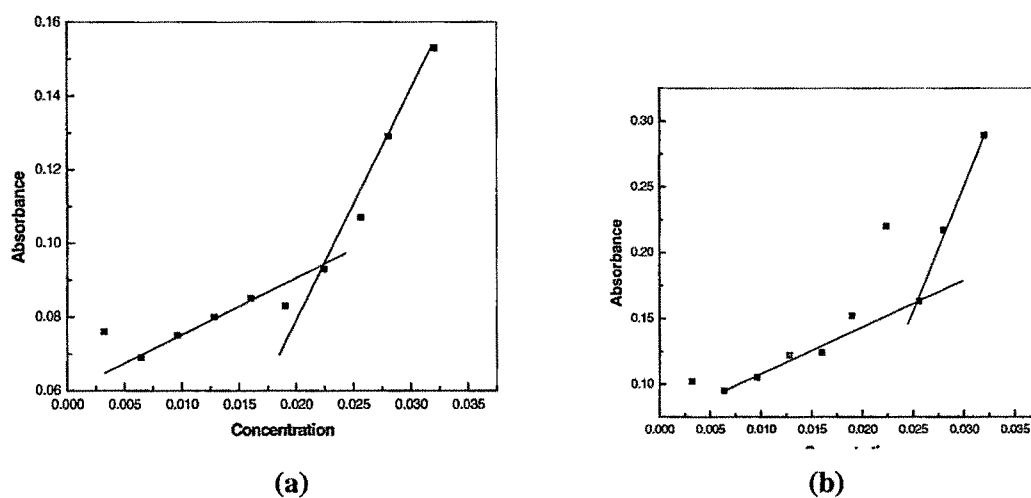


**Figure 3.7.** Plot of absorbance Vs. concentration of Brij 35 in the presence of [60]fullerene to determine cmc at (a) 30°C and (b) 40°C.

**Table 3.2** Critical reverse micelle concentration, free energy, enthalpy and entropy of reverse micellization of Brij35 in toluene-[60]fullerene solution at 30°C and 40°C.

Temperature	Crmc	$-\Delta G_{rm}^{\circ}$	$-\Delta H_{rm}^{\circ}$	$-\Delta S_{rm}^{\circ}$
°C	mmol dm <sup>-3</sup>	kJmol <sup>-1</sup>	kJmol <sup>-1</sup>	J mol <sup>-1</sup> k <sup>-1</sup>
30	0.0209	96.10	286.07	0.610
40	0.0253	103.41	366.59	0.767

### 3.2.2 Microemulsion formation

A clear microemulsion was formed in non-ionic surfactant-[60]fullerene system using propanol as a co-surfactant. The present studies indicate that [60]fullerene is stable in the microemulsion form in pure as well as in mixed surfactant systems. The presence of [60]fullerene increases the water required for the formation of the microemulsion and reduces as the ratio of toluene/propanol increases. The values are summarized in the Table 3.3(a) and Table 3.3(b). At a fixed quantity of the oil component ie toluene and the surfactant Span 60, the cosurfactant concentration was varied from 1 ml to 5ml and the water required for the transition from the microemulsion (clear region) to the emulsion (turbid region) was measured by successive titrations by addition of 0.02 ml water. These values are shown in the Table 3.3 (a) and Table 3.3(b). Which is having the observations in the presence as well absence of [60]fullerene. In the table the point wise observations were recorded and final point was decided when the solution becomes turbid.

**Table 3.3(a). Effect of variation of amount of cosurfactant on the nature of solution**

Toluene (ml)	Surfactant (gm)	Cosurfactant (ml)	Water titration (ml)	Solution
5.0	0.068 (Span 60)	1.0 (propanol)	0.02	Clear
			0.04	Clear
			0.06	Clear
			0.08	Clear
			0.09	Turbid
		2.0		Clear
			0.10	Clear
			0.15	Clear
			0.17	Clear
			0.19	Clear
			0.21	Turbid
		3.0		Clear
			0.23	Clear
			0.25	Clear
			0.30	Clear
			0.35	Clear
			0.38	Clear
			0.42	Turbid
		4.0		Clear
			0.45	Clear
			0.50	Clear
			0.55	Clear
			0.60	Clear
			0.62	Clear
			0.65	Turbid
		5.0		Clear
			0.70	Clear
			0.75	Clear
			0.80	Clear
			0.85	Turbid



**Table 3.3(b). Effect of variation of amount of cosurfactant on the nature of solution in presence of [60]fullerene**

Toluene+[60]full (ml)	Surfactant (gm)	Cosurfactant (ml)	Water titration (ml)	Solution
5.0	0.068 (Span 60)	1.0 (propanol)	0.02	Clear
			0.04	Clear
			0.06	Clear
			0.08	Clear
			0.09	Clear
			0.11	Clear
			0.13	Turbid
		2.0		Clear
			0.15	Clear
			0.20	Clear
			0.23	Turbid
		3.0		Clear
			0.25	Clear
			0.30	Clear
			0.35	Clear
			0.40	Clear
			0.41	Turbid
		4.0		Clear
			0.45	Clear
			0.50	Clear
			0.55	Clear
			0.60	Clear
			0.65	Turbid
		5.0		Clear
			0.70	Clear
			0.75	Clear
			0.80	Clear
			0.85	Clear
			0.90	Clear
			0.95	Clear
			0.98	Turbid

Based on these values it is found that the presence of more amount of the cosurfactant enhances the water content of the microemulsion. This is shown graphically in the Figure 3.8.

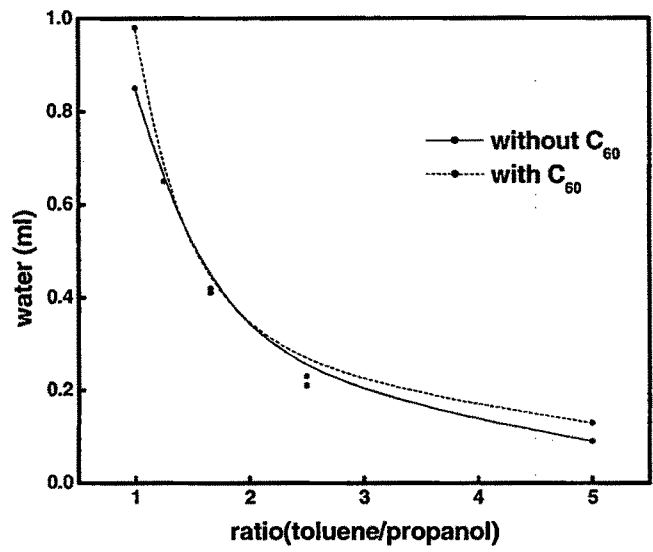


**Figure 3.8.** Water consumed versus ratio of toluene/propanol in [60]fullerene (2ml)-Span60 Systems.

### 3.2.2.1 Effect of Various Surfactants and Co-Surfactants

The effect of the variation of the surfactant type as well as the amount of cosurfactant on the formation of microemulsion was also measured using the same method as mentioned before. The results of these titrations where the transition from the microemulsion to the emulsion takes place are given in Table 3.4(a) for Span 60 and Table 3.4(b) for Span 20.

**Table 3.4(a). Effect of variation of the surfactant Span 60 and cosurfactant quantity on the nature of solution**

Toluene (ml)	Surfactant (gm)	Cosurfactant (ml)	Water titration (ml)	Solution
5.0	0.068 (Span 60)	1.0 (propanol)	0.02	Clear
			0.04	Clear
			0.06	Clear
			0.08	Clear
			0.09	Turbid
		2.0		Clear
			0.10	Clear
			0.15	Clear
			0.17	Clear
			0.19	Clear
			0.21	Turbid
		3.0		Clear
			0.23	Clear
			0.25	Clear
			0.30	Clear
			0.35	Clear
			0.38	Clear
			0.42	Turbid
		4.0		Clear
			0.45	Clear
			0.50	Clear
			0.55	Clear
			0.60	Clear
			0.62	Clear
			0.65	Turbid
		5.0		Clear
			0.70	Clear
			0.75	Clear
			0.80	Clear
			0.85	Turbid

Toluene (ml)	Surfactant (gm)	Cosurfactant (ml)	Water titration (ml)	Solution
5.0	0.068 (Span 60)	1.0 (butanol)	0.02	Clear
			0.04	Clear
			0.06	Clear
			0.07	Turbid
		2.0		Clear
			0.10	Clear
			0.13	Clear
			0.15	Turbid
		3.0		Clear
			0.20	Clear
			0.22	Turbid
		4.0		Clear
			0.25	Clear
			0.30	Clear
			0.33	Turbid
		5.0		Clear
			0.35	Clear
			0.40	Clear
			0.45	Clear
			0.47	Turbid

Toluene (ml)	Surfactant (gm)	Cosurfactant (ml)	Water titration (ml)	Solution
5.0	0.068 (Span60)	1.0 (pentanol)	0.02	Clear
			0.04	Clear
			0.06	Clear
			0.07	Turbid
		2.0		Clear
			0.10	Clear
			0.12	Turbid
		3.0		Clear
			0.14	Clear
			0.16	Turbid
		4.0		Clear
			0.20	Clear
			0.25	Clear
			0.28	Turbid
		5.0		Clear
			0.30	Clear
			0.35	Clear
			0.38	Turbid

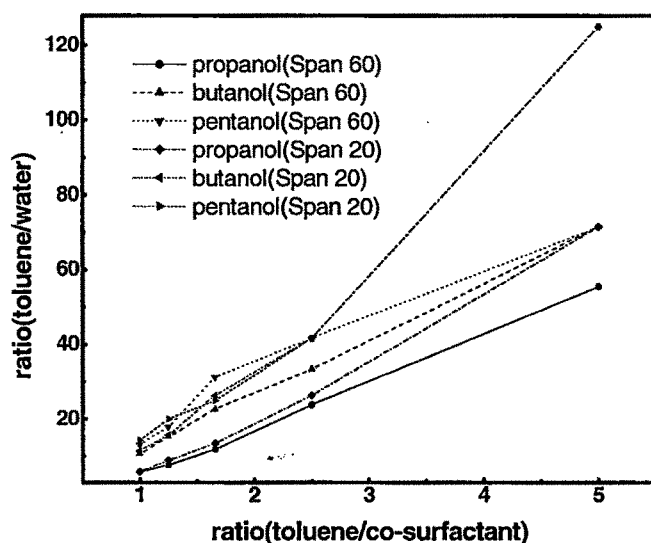
**Table 3.4(b) Effect of variation of the surfactant Span 20 and cosurfactant quantity on the nature of solution**

Toluene (ml)	Surfactant (gm)	Cosurfactant (ml)	Water titration (ml)	Solution
5.0	0.068 (Span 20)	1.0 (propanol)	0.02	Clear
			0.04	Clear
			0.06	Clear
			0.08	Clear
			0.09	Turbid
		2.0		Clear
			0.10	Clear
			0.15	Clear
			0.17	Clear
			0.19	Turbid
		3.0		Clear
			0.21	Clear
			0.23	Clear
			0.25	Clear
			0.30	Clear
			0.35	Clear
			0.37	Turbid
		4.0		Clear
			0.40	Clear
			0.45	Clear
			0.50	Clear
			0.56	Turbid
		5.0		Clear
			0.60	Clear
			0.65	Clear
			0.70	Clear
			0.75	Clear
			0.80	Clear
			0.86	Turbid

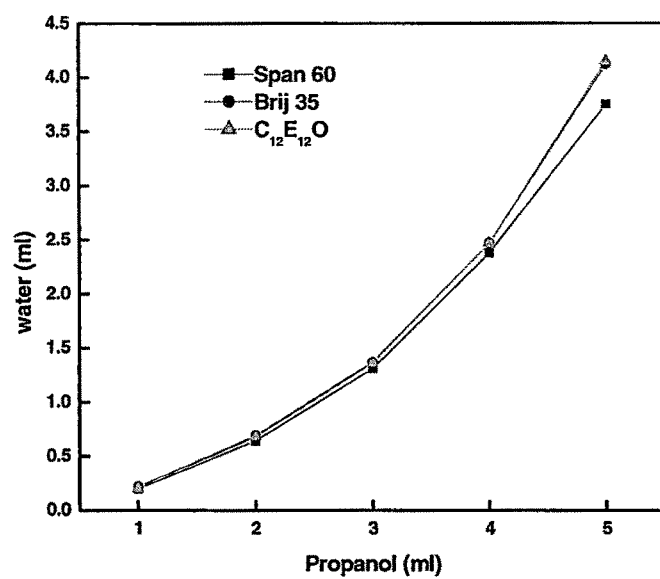
Toluene(ml)	Surfactant (gm)	Cosurfactant (ml)	Water titration (ml)	Solution
5.0	0.068 (Span 20)	1.0 (Butanol)	0.02	Clear
			0.04	Turbid
		2.0		Clear
			0.05	Clear
			0.10	Clear
			0.12	Clear
		3.0		Clear
			0.15	Clear
			0.17	Clear
			0.19	Turbid
		4.0		Clear
			0.22	Clear
			0.25	Clear
			0.30	Clear
			0.32	Turbid
		5.0		Clear
			0.35	Clear
			0.40	Clear
			0.44	Turbid

Toluene (ml)	Surfactant (gm)	Cosurfactant (ml)	Water titration (ml)	Solution
5.0	0.068 (Span 20)	1.0 (Pentanol)	0.02	Clear
			0.04	Turbid
		2.0		Clear
			0.06	Clear
			0.08	Clear
			0.10	Clear
			0.12	Turbid
		3.0		Clear
			0.15	Clear
			0.18	Clear
			0.20	Turbid
		4.0		Clear
			0.22	Clear
			0.25	Turbid
		5.0		Clear
			0.30	Clear
			0.35	Turbid

Figure 3.9 shows the effect of the change in the ratio of the toluene/cosurfactant on the water consumption for the formation of the emulsion. As the cosurfactant is changed from propanol to butanol to pentanol there is decrease in water consumption. Thus as the polar nature of the cosurfactant reduces i.e. the carbon chain increases the water required for the formation of the emulsion is decreased. When the surfactant is changed from Span 20 to Span 60 not much change is observed. It was also observed that when the surfactant was changed to Brij 35 then the water required for the emulsion formation was higher [Figure.3.10]. This is clearly evident from the structural difference between the Span type of surfactant and the Brij type of surfactant. The structure of the surfactant does have a major role to play in the formation of the emulsion and these are given in Table 3.5.



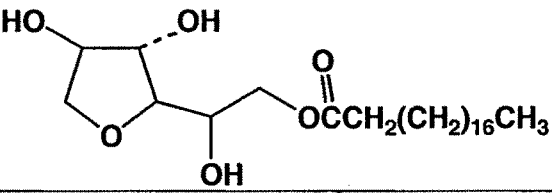
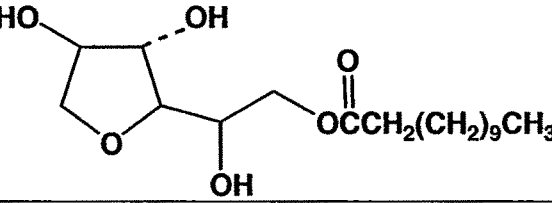
**Figure 3.9.** Plot of the effect of change in the ratio of the toluene/cosurfactant on the formation of the microemulsion.



**Figure 3.10.** Plot of effect of change in Surfactant on the quantity of water required for emulsion formation at different concentrations of cosurfactant (propanol)



**Table 3.5. Structures of different non-ionic surfactants used in the present study.**

Name	Structure
Span 60	
Span 20	
Brij 35	$\text{CH}_3(\text{CH}_2)_{11}(\text{OCH}_2\text{CH}_2)_{23}\text{OH}$ MW~1199
Brij 98	$\text{C}_{18}\text{H}_{35}(\text{OCH}_2\text{CH}_2)_{20}\text{OH}$ (MW~1150)
$\text{C}_{12}\text{E}_{12}\text{O}$	$\text{C}_{12}\text{H}_{25}(\text{OCH}_2\text{CH}_2)_{12}\text{OH}$

### 3.2.2.2 Effect of change in concentration of solvent

It was observed that if we decrease the amount of solvent (toluene) in the system then more water is required for emulsion formation. These observations were recorded using the titration method. In which the concentration of the toluene was changed by changing the total amount of the toluene 5ml, 2ml, 1ml. Variation in the amount of water required for the emulsion formation was recorded at fixed quantity of the oil component and the surfactant i.e. span60 and the concentration of the co surfactant was varied from 1ml to 5ml. All the recorded values were summarized in the Table 3.6 and all these observations were made in the absence of [60]fullerene. The clear change in the final reading (i.e turbid region recorded at each 1ml addition of the propanol) was observed as we change the concentration of the Toluene from 5ml, 2ml to 1ml. It is seen that when amount of toluene is 5.0ml then water required for the emulsion formation with 5.0ml, of the cosurfactant (propanol) is 0.85ml. Similarly when toluene is 2.0ml then 1.67ml and at 1.0ml of toluene water required for the emulsion formation is 3.75ml. These observations reveal that at low concentration of the solvent more water is required.

**Table 3.6. Effect of variation of ratio of oil/cosurfactant on nature of solution**

Toluene (ml)	Surfactant (gm)	Cosurfactant (ml)	Water titration (ml)	Solution
<b>5.0</b>	<b>0.085(Span 60)</b>	<b>1.0 (propanol)</b>	0.02	Clear
			0.04	Clear
			0.06	Clear
			0.08	Clear
			0.09	Turbid
		2.0		Clear
			0.10	Clear
			0.15	Clear
			0.17	Clear
			0.19	Clear
			0.21	Turbid
		3.0		Clear
			0.23	Clear
			0.25	Clear
			0.30	Clear
			0.35	Clear
			0.38	Clear
			0.42	Turbid
		4.0		Clear
			0.45	Clear
			0.50	Clear
			0.55	Clear
			0.60	Clear
			0.62	Clear
			0.65	Turbid
		5.0		Clear
			0.70	Clear
			0.75	Clear
			0.80	Clear
			0.85	Turbid

Toluene (ml)	Surfactant (gm)	Cosurfactant (ml)	Water titration (ml)	Solution
2.0	0.085(Span 60)	1.0 (propanol)	0.02	Clear
			0.04	Clear
			0.06	Clear
			0.08	Clear
			0.10	Turbid
		2.0		Clear
			0.10	Clear
			0.15	Clear
			0.20	Clear
			0.25	Clear
			0.30	Clear
			0.35	Clear
			0.37	Turbid
		3.0		Clear
			0.40	Clear
			0.45	Clear
			0.50	Clear
			0.55	Clear
			0.60	Clear
			0.65	Clear
			0.69	Turbid
		4.0		Clear
			0.75	Clear
			0.80	Clear
			0.90	Clear
			1.0	Clear
			1.1	Turbid
		5.0		Clear
			1.2	Clear
			1.3	Clear
			1.4	Clear
			1.5	Clear
			1.6	Clear
			1.67	Turbid

Toluene (ml)	Surfactant (gm)	Cosurfactant (ml)	Water titration (ml)	Solution
1.0	0.085 (Span 60)	1.0 (propanol)	0.05	Clear
			0.10	Clear
			0.12	Clear
			0.15	Clear
			0.2	Turbid
		2.0		Clear
			0.3	Clear
			0.4	Clear
			0.5	Clear
			0.55	Clear
			0.6	Clear
			0.64	Turbid
		3.0		Clear
			0.7	Clear
			0.8	Clear
			0.9	Clear
			1.0	Clear
			1.1	Clear
			1.2	Clear
			1.25	Clear
			1.31	Turbid
		4.0		Clear
			1.4	Clear
			1.6	Clear
			1.8	Clear
			2.0	Clear
			2.2	Clear
			2.25	Clear
			2.30	Clear
			2.35	Clear
			2.38	Turbid
		5.0		Clear
			2.5	Clear
			2.8	Clear
			3.0	Clear
			3.2	Clear
			3.4	Clear
			3.6	Clear
			3.65	Clear
			3.7	Clear
			3.75	Turbid

From the Figure 3.11 we can clearly observe the significant increase in water amount with decrease in toluene amount from 5ml to 1ml.

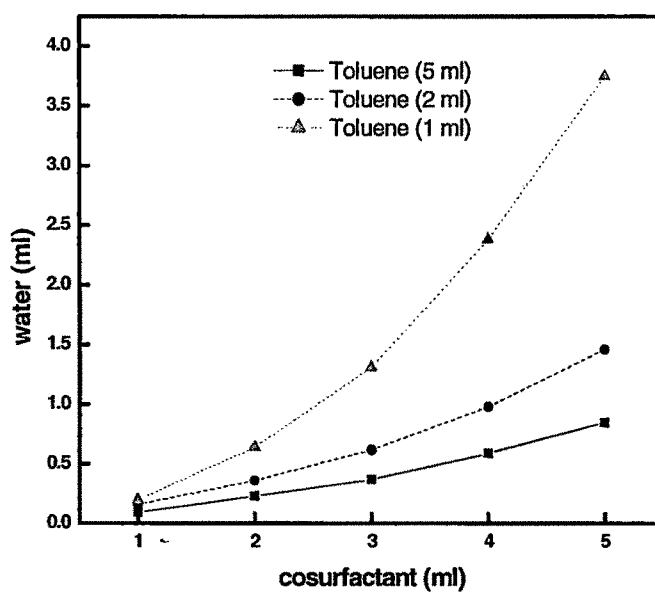


**Figure 3.11.** Plot of effect of change in toluene quantity on the quantity of water required foremulsion formation at different concentrations of cosurfactant (propanol).

### 3.2.2.3 Phase behavior study

Based on the results obtained previously, triangular phase diagrams were drawn for the microemulsion systems using water titration method. Table 3.7(a-b) contains the solubility data of toluene with and without [60]fullerene solution in toluene and water with Span 60+Propanol, at 30°C. From all the titration values recorded in the table we can clearly see that in the presence of [60]fullerene, less amount of the Span 60-Propanol solution is required compared to in the absence of [60]fullerene. These observation says that [60]fullerene helps in the microemulsion formation. Similar observations were obtained in case of Brij35, Brij98, C<sub>12</sub>E<sub>12</sub>O as well as for mixed surfactant system. Tables containing miscibility data of all surfactants are shown in the Tables 3.8-3.14. Based on these values the ternary plot for all the surfactants and the surfactant mixture were drawn. These are shown in Figures 3.12 to Figure 3.18 where the weight fractions of components were plotted.

**Table 3.7(a). Solubility data of Toluene and water with Span 60+ Propanol, at 30°C**

Water (ml)	Toluene (ml)	Span 60-Propanol (ml)	Solution
1.0	0.3	3.0	Clear
1.0	0.5	3.49	Clear
1.0	0.7	4.24	Clear
1.0	0.9	4.52	Clear
1.0	1.1	4.92	Clear
1.0	1.3	5.3	Clear
1.0	1.5	5.95	Clear
1.0	1.7	6.04	Clear
1.0	1.9	6.28	Clear
1.0	2.1	6.8	Clear
1.0	2.3	7.88	Clear
1.0	2.5	8.0	Clear
1.0	2.7	7.54	Clear
1.0	2.9	7.88	Clear

**Table 3.7(b). Solubility data of [60]fullerene solution in Toluene and water with Span 60+ Propanol, at 30°C**

Water (ml)	C <sub>60</sub> solution (ml)	Span 60-Propanol (ml)	Solution
1.0	0.3	2.8	Clear
1.0	0.5	3.62	Clear
1.0	0.7	4.24	Clear
1.0	0.9	4.98	Clear
1.0	1.1	5.51	Clear
1.0	1.3	5.94	Clear
1.0	1.5	6.12	Clear
1.0	1.7	6.3	Clear
1.0	1.9	6.54	Clear
1.0	2.1	6.82	Clear
1.0	2.3	7.12	Clear
1.0	2.5	7.22	Clear
1.0	2.7	7.3	Clear
1.0	2.9	7.7	Clear



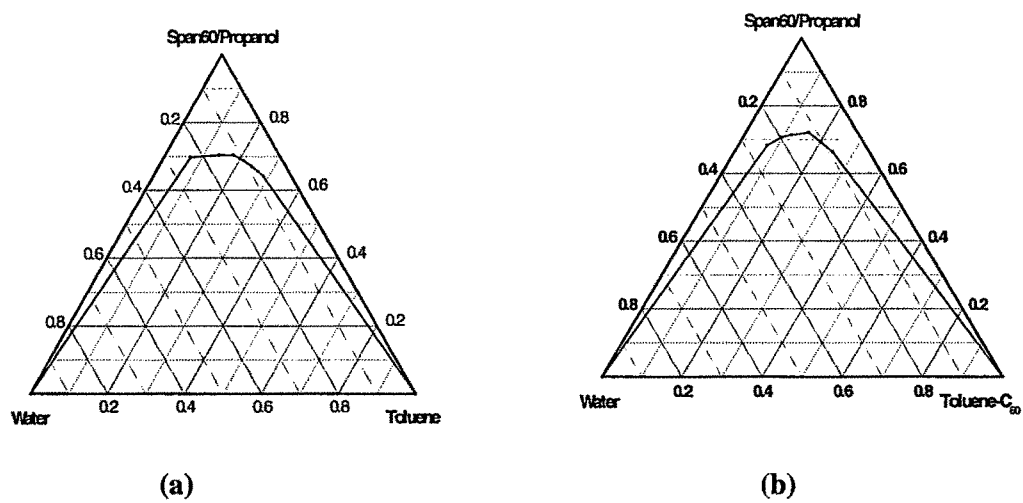


**Figure 3.12.** Triangular phase diagram for Span 60 in (a) absence of fullerene and (b) presence of [60]fullerene.

**Table 3.8(a). Miscibility data of Toluene and water with surfactant Brij 35 + Propanol at 30°C.**

Water (ml)	Toluene (ml)	Brij 35 + Propanol (ml)	Solution
1.0	0.1	0.44	Clear
1.0	0.3	1.28	Clear
1.0	0.5	1.91	Clear
1.0	0.7	2.4	Clear
1.0	0.9	2.69	Clear
1.0	1.1	3.4	Clear
1.0	1.3	3.26	Clear
1.0	1.5	3.61	Clear
1.0	1.7	3.78	Clear
1.0	1.9	4.05	Clear
1.0	2.1	4.22	Clear
1.0	2.3	4.46	Clear
1.0	2.5	4.6	Clear
1.0	2.7	4.85	Clear
1.0	2.9	5.28	Clear

**Table 3.8(b). Miscibility data of C<sub>60</sub> solution and water with surfactant Brij 35+Propanol at 30°C**

Water (ml)	C <sub>60</sub> Solution (ml)	Brij 35 + Propanol (ml)	Solution
1.0	0.1	0.48	Clear
1.0	0.3	1.34	Clear
1.0	0.5	1.9	Clear
1.0	0.7	2.38	Clear
1.0	0.9	2.78	Clear
1.0	1.1	3.06	Clear
1.0	1.3	3.45	Clear
1.0	1.5	3.58	Clear
1.0	1.7	3.78	Clear
1.0	1.9	4.19	Clear
1.0	2.1	4.36	Clear
1.0	2.3	4.7	Clear
1.0	2.5	4.92	Clear
1.0	2.7	5.12	Clear
1.0	2.9	5.21	Clear

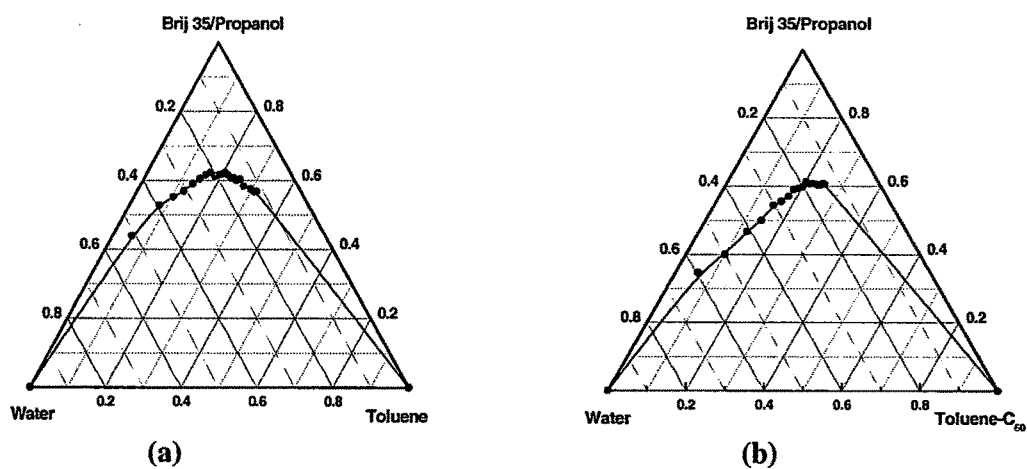


**Figure 3.13** Triangular phase diagram for Brij35 surfactant in (a) absence of [60]fullerene and (b) presence of [60]fullerene.

**Table3.9(a). Miscibility data of toluene and water with surfactant Brij 98+Propanol at 30°C**

Water(ml)	Toluene(ml)	Brij98-Propanol (ml)	Solution
1.0	0.1	0.39	Clear
1.0	0.2	0.53	Clear
1.0	0.3	1.36	Clear
1.0	0.4	1.91	Clear
1.0	0.5	2.13	Clear
1.0	0.6	2.46	Clear
1.0	0.7	2.76	Turbid
1.0	0.8	2.73	Clear
1.0	0.9	3.11	Clear
1.0	1.0	3.12	Clear
1.0	1.1	3.43	Clear
1.0	1.2	3.53	Clear
1.0	1.3	3.76	Clear
1.0	1.4	3.96	Clear

**Table3.9(b). Miscibility data of C<sub>60</sub> solution and water with surfactant Brij 98+Propanol at 30°C**

Water(ml)	C <sub>60</sub> solution (ml)	Brij 98-Propanol (ml)	Solution
1.0	0.1	0.38	Clear
1.0	0.2	1.12	Clear
1.0	0.3	1.73	Clear
1.0	0.4	2.0	Clear
1.0	0.5	2.3	Clear
1.0	0.6	2.77	Clear
1.0	0.7	2.6	Turbid
1.0	0.8	3.12	Clear
1.0	0.9	3.24	Clear
1.0	1.0	3.29	Clear
1.0	1.1	3.47	Clear
1.0	1.2	3.51	Clear
1.0	1.3	3.78	Clear
1.0	1.4	4.0	Clear
1.0	1.4	4.45	Clear

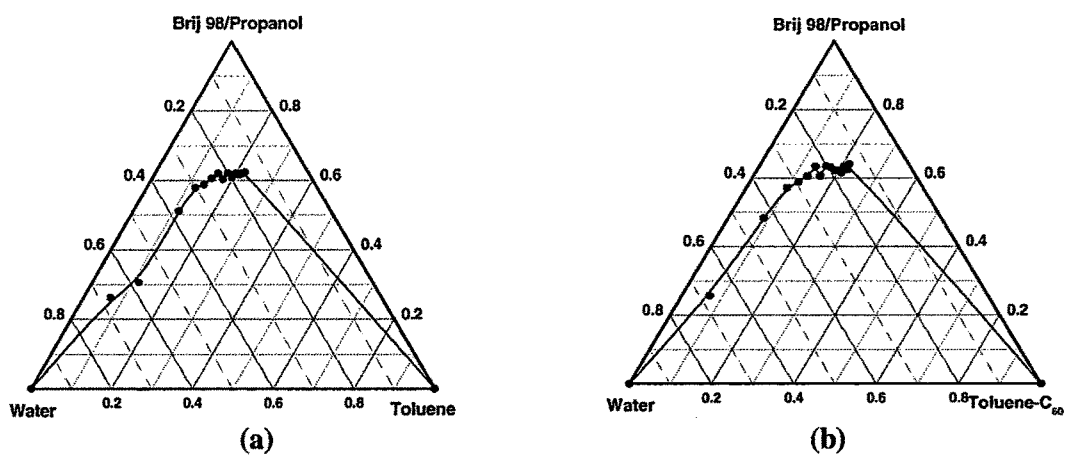


**Figure 3.14** Triangular phase diagram for Brij 98 surfactant in (a) absence of [60]fullerene and (b) presence of [60]fullerene.

**Table 3.10(a). Miscibility data of toluene and water with surfactant C<sub>12</sub>E<sub>12</sub>O at 30°C**

Water(ml)	Toluene(ml)	C <sub>12</sub> E <sub>12</sub> O-Propanol (ml)	Solution
1.0	0.1	0.85	Clear
1.0	0.2	1.41	Clear
1.0	0.3	1.89	Clear
1.0	0.4	2.13	Clear
1.0	0.5	2.68	Clear
1.0	0.6	2.9	Clear
1.0	0.7	2.98	Turbid
1.0	0.8	3.43	Clear

**Table 3.10(b). Miscibility data of C<sub>60</sub> solution and water with surfactant C<sub>12</sub>E<sub>12</sub>O at 30°C**

Water(ml)	C <sub>60</sub> solution (ml)	C <sub>12</sub> E <sub>12</sub> O-Propanol (ml)	Solution
1.0	0.1	0.38	Clear
1.0	0.2	1.24	Clear
1.0	0.3	1.79	Clear
1.0	0.4	2.35	Clear
1.0	0.5	2.6	Clear
1.0	0.6	2.75	Clear
1.0	0.7	3.1	Turbid
1.0	0.8	3.21	Clear

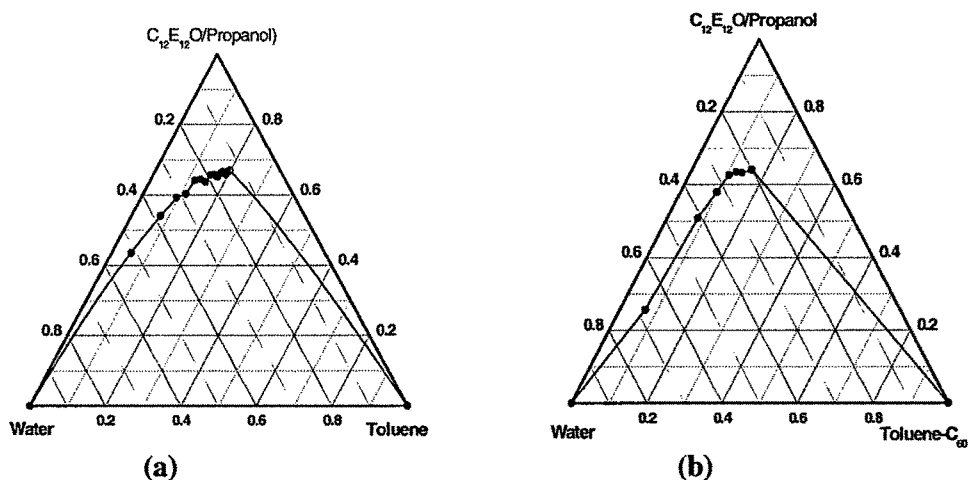


**Figure 3.15** Triangular phase diagram for  $C_{12}E_{12}O$  in (a) absence of [60]fullerene and (b) presence of [60]fullerene.

In all these Figures (3.12-3.18) the upper portion is the monophasic microemulsion region ( $1\phi$ ). The lower portion is the liquid/liquid (L/L) biphasic region ( $2\phi$ ). In the biphasic region the microemulsion is in equilibrium with excess oil (toluene). The areas under the curve as well as upper area of the curve were calculated using digital planimeter (Koizumi, PLA COM, KP-90) with accuracy of  $\pm 0.2\%$ . Using Span 60 as a surfactant, the triangular phase diagram was drawn and is shown in the Figure 3.12. The value obtained for the area of monophasic microemulsion region in the absence of [60]fullerene was  $2.4 \text{ cm}^2$  while in the presence of [60]fullerene was  $3.1 \text{ cm}^2$ . In case of Brij 35 and Brij 98 in the absence of [60]fullerene the area calculated was found to be  $3.4 \text{ cm}^2$ ,  $4.6 \text{ cm}^2$  respectively and in the presence of [60]fullerene  $4.2 \text{ cm}^2$  and  $4.8 \text{ cm}^2$  respectively. Thus in both the case of Brij 35 and Brij 98 the area under the curve is more in the presence of fullerene. Similarly the ternary plot was drawn using  $C_{12}E_{12}O$  as a nonionic surfactant and area of the monophasic microemulsion region calculated and was found to be  $3.1 \text{ cm}^2$  in the absence of [60]fullerene and  $4.3 \text{ cm}^2$  in the presence of [60]fullerene. These studies using different non-ionic surfactant indicate that in the presence of [60]fullerene area of the monophasic microemulsion region was increased compared to in the absence of [60]fullerene. This monophasic microemulsion region contains only one phase and so is clear that in the presence of [60]fullerene water phase

increased. However the phase diagram remained reasonably unchanged for the systems at high temperature.

#### **3.4.2.4 Effect of change in Temperature on phase behaviour**

Here microemulsions were formed from the fullerene-toluene solution and water using structurally different surfactants like Brij 35 and Span 60 and their phase behavior was studied at 30 °C and 40°C and is observed that with change in temperature, area of the monophasic microemulsion system also changed. Area of the upper portion [monophasic microemulsion region (1 $\phi$ )] and the lower portion [biphasic region (2 $\phi$ )] was calculated using digital planimeter at both temperatures. In case of Span 60-[60]fullerene microemulsion system the area of monophasic microemulsion region (1 $\phi$ ) was found to be 3.1 cm<sup>2</sup> at 30°C, 3.3 cm<sup>2</sup> at 40°C and 3.6 cm<sup>2</sup> at 50°C so clearly it seems that at higher temperature the area of the monophasic microemulsion region was increased. Same was the trend observed in case of structurally different non-ionic surfactant Brij 35 and the area increased from 4.2 cm<sup>2</sup> at 30 °C to 4.4 cm<sup>2</sup> at 40 °C.



**Table 3.11(a-1). Solubility data of toluene and water with Span 60+Propanol, at 40°C.**

Water (ml)	Toluene (ml)	Span 60- Propanol (ml)	Solution
1.0	0.1	2.88	Clear
1.0	0.3	2.66	Clear
1.0	0.5	3.24	Clear
1.0	0.7	3.94	Clear
1.0	0.9	4.26	Clear
1.0	1.1	4.56	Clear
1.0	1.3	5.1	Clear
1.0	1.5	5.22	Clear
1.0	1.7	5.92	Clear
1.0	1.9	6.08	Clear
1.0	2.1	6.48	Clear
1.0	2.3	6.82	Clear
1.0	2.5	7.3	Clear
1.0	2.7	7.3	Clear
1.0	2.9	7.76	Clear
1.0	3.1	8.04	Clear
1.0	3.3	8.18	Clear
1.0	3.5	8.66	Clear
1.0	3.7	8.92	Clear
1.0	3.9	9.05	Clear

**Table 3.11(a-2). Solubility data of [60]fullerene solution in toluene and water with Span 60+Propanol, at 40°C.**

Water (ml)	C <sub>60</sub> solution (ml)	Span 60-Propanol (ml)	Solution
1.0	0.1	2.5	Clear
1.0	0.3	2.7	Clear
1.0	0.5	3.2	Clear
1.0	0.7	4.36	Clear
1.0	0.9	4.28	Clear
1.0	1.1	4.77	Clear
1.0	1.3	4.98	Clear
1.0	1.5	5.62	Clear
1.0	1.7	5.92	Clear
1.0	1.9	6.36	Clear
1.0	2.1	6.6	Clear
1.0	2.3	6.9	Clear
1.0	2.5	7.3	Clear
1.0	2.7	7.46	Clear
1.0	2.9	7.94	Clear
1.0	3.1	8.18	Clear
1.0	3.3	8.24	Clear

**Table 3.11(b-1). Solubility data of toluene and water with Span 60+Propanol, at 50°C.**

Water (ml)	Toluene (ml)	Span 60-Propanol (ml)	Solution
1.0	0.1	2.21	Clear
1.0	0.3	2.79	Clear
1.0	0.5	3.5	Clear
1.0	0.7	3.97	Clear
1.0	0.9	4.42	Clear
1.0	1.1	5.14	Clear
1.0	1.3	5.35	Clear
1.0	1.5	5.4	Clear
1.0	1.7	5.52	Clear
1.0	1.9	5.96	Clear
1.0	2.1	6.5	Clear
1.0	2.3	6.7	Clear
1.0	2.5	7.36	Clear
1.0	2.7	6.9	Clear
1.0	2.9	7.32	Clear
1.0	3.1	7.51	Clear
1.0	3.3	7.9	Clear
1.0	3.5	8.04	Clear
1.0	3.7	8.14	Clear
1.0	3.9	8.3	Clear

**Table 3.11(b-2). Solubility data of [60]fullerene solution in toluene and water with Span 60+Propanol, at 50°C**

Water (ml)	C <sub>60</sub> solution (ml)	Span 60-Propanol (ml)	Solution
1.0	0.1	3.16	Clear
1.0	0.3	2.92	Clear
1.0	0.5	3.32	Clear
1.0	0.7	3.9	Clear
1.0	0.9	4.3	Clear
1.0	1.1	4.8	Clear
1.0	1.3	5.12	Clear
1.0	1.5	5.76	Clear
1.0	1.7	5.88	Clear
1.0	1.9	6.36	Clear
1.0	2.1	6.96	Clear
1.0	2.3	6.96	Clear
1.0	2.5	7.27	Clear
1.0	2.7	7.0	Clear
1.0	2.9	7.5	Clear
1.0	3.1	8.02	Clear
1.0	3.3	8.1	Clear

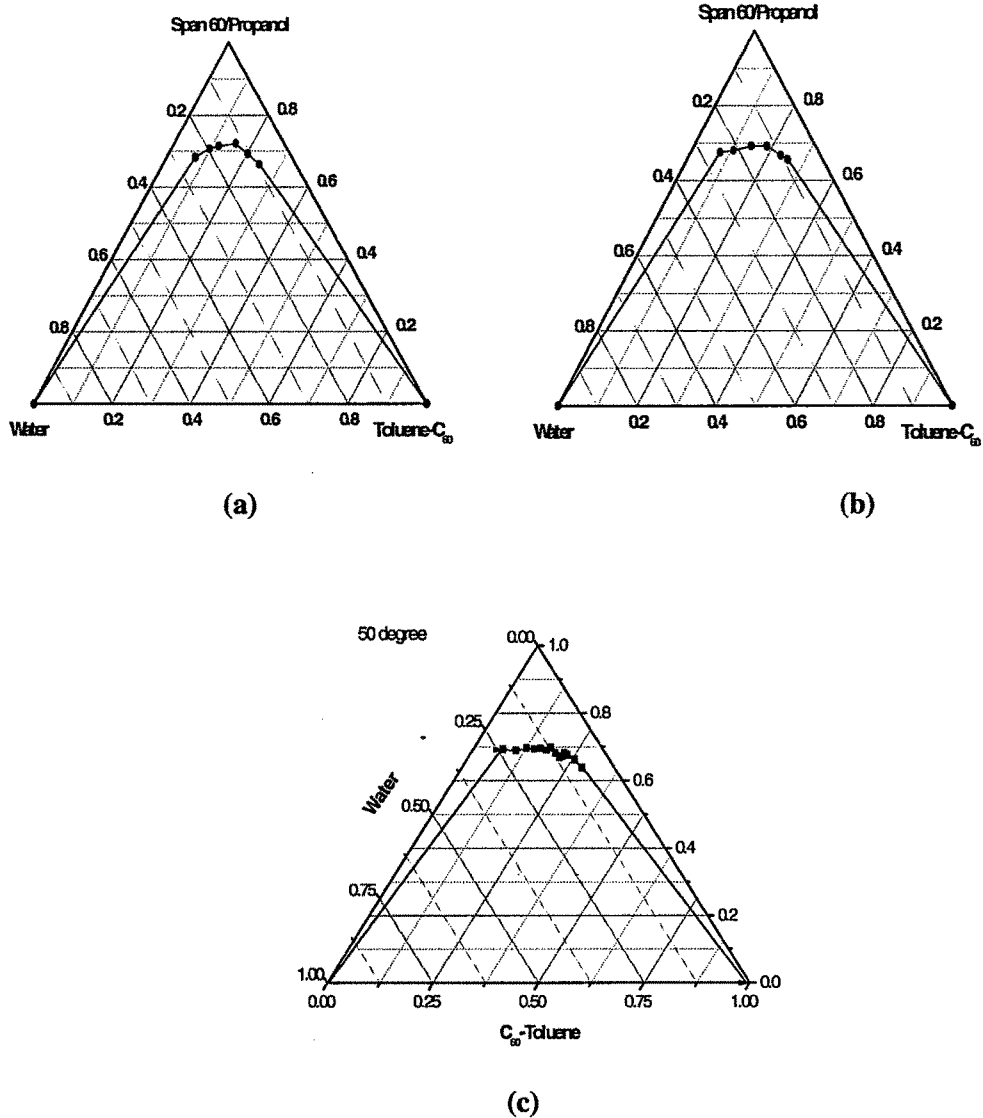


**Figure 3.16** Triangular phase diagram for Span 60 surfactant in the presence of [60]fullerene (a) at 30 °C and (b) 40 °C (c) 50 °C

**Table 3.12(a). Miscibility data of Toluene and water with surfactant Brij 35+Propanol at 40°C.**

Water(ml)	Toluene (ml)	Brij 35 + Propanol (ml)	Solution
1.0	0.1	0.84	Clear
1.0	0.3	1.52	Clear
1.0	0.5	1.94	Clear
1.0	0.7	2.4	Clear
1.0	0.9	2.61	Clear
1.0	1.1	3.04	Clear
1.0	1.3	3.26	Clear
1.0	1.5	3.42	Clear
1.0	1.7	3.8	Turbid
1.0	1.9	3.86	Clear
1.0	2.1	4.08	Clear
1.0	2.3	4.28	Clear
1.0	2.5	4.48	Clear
1.0	2.7	4.62	Clear
1.0	2.9	4.64	Clear
1.0	3.1	4.94	Clear
1.0	3.5	5.34	Clear
1.0	3.7	5.28	Clear
1.0	3.9	5.42	Clear
1.0	4.1	6.2	Clear

**Table 3.12(b). Miscibility data of C<sub>60</sub> solution and water with surfactant Brij 35+Propanol at 40°C.**

Water (ml)	C <sub>60</sub> solution (ml)	Brij 35-Propanol (ml)	Solution
1.0	0.1	0.36	Clear
	0.3	1.04	Clear
	0.5	1.7	Clear
	0.7	2.14	Clear
	0.9	2.54	Clear
	1.1	2.86	Clear
	1.3	3.3	Clear
	1.5	3.54	Clear
	1.7	3.7	Clear
	1.9	4.04	Clear
	2.1	4.12	Clear
	2.3	4.4	Clear
	2.5	4.66	Clear
	2.7	4.58	Clear
	2.9	4.6	Clear
	3.1	4.88	Clear
	3.3	4.96	Clear
	3.5	5.2	Clear
	3.7	5.32	Clear
	3.9	5.46	Clear
	4.1	6.22	Clear
	4.5	6.06	Clear
	4.9	6.49	Clear

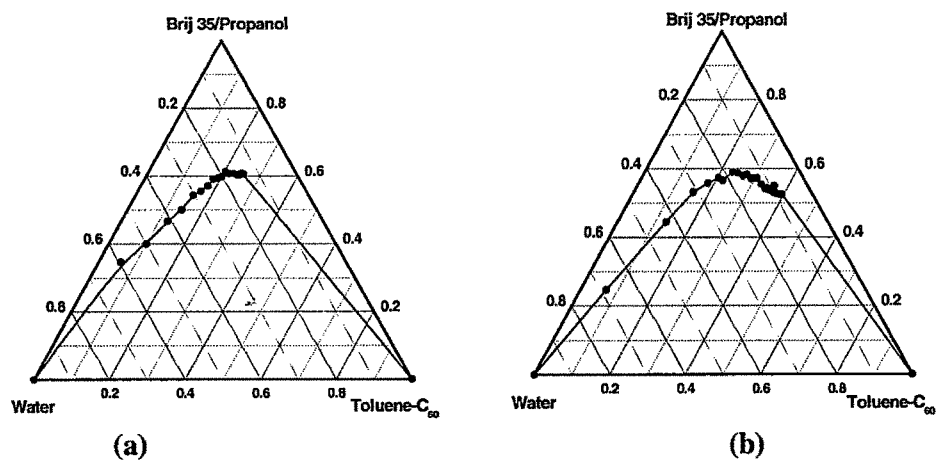


**Figure 3.17.** Triangular phase diagram for Brij 35 surfactant in the presence of [60]fullerene at (a)30 °C and (b)40 °C.





#### 3.4.2.5. Mixed Surfactant Study

After studying the phase behavior using single non-ionic surfactant it was thought to study phase behavior of these same non-ionic surfactants in the mixture form. The surfactants used were Brij 35 and  $C_{12}E_{12}O$  as they are structurally similar and are long chain surfactants. The phase behavior was studied in the presence as well absence of [60]fullerene and the ternary plots were drawn and are shown in the Figure 3.18. Again the area of both the regions were calculated to understand the behavior of mixed surfactant system and in the absence of [60]fullerene the area of monophasic microemulsion region was found to be  $3.4 \text{ cm}^2$  while in the presence of [60]fullerene was  $4.2 \text{ cm}^2$ . This change was same as was observed if we used single surfactant system so it seems that there was not much change observed if we use mixed surfactant system on the microemulsion formation. Generally it was observed that mixed surfactant system is better than that of the single surfactant but it is not as effective in the case of [60]fullerene.

**Table 3.13(a) . Solubility data of Toluene and water with mixed surfactant Brij 35+ C<sub>12</sub>E<sub>12</sub>O at 30°C.**

Water (ml)	Toluene (ml)	Brij 35+C <sub>12</sub> E <sub>12</sub> O/ Propanol (ml)	Solution
1.0	0.1	0.76	Clear
1.0	0.2	1.12	Clear
1.0	0.3	1.55	Clear
1.0	0.4	1.9	Clear
1.0	0.5	2.31	Clear
1.0	0.6	2.74	Clear
1.0	0.7	2.89	Turbid
1.0	0.8	2.95	Clear

**Table 3.13(b). Solubility data of C<sub>60</sub> solution and water with mixed surfactant Brij 35+C<sub>12</sub>E<sub>12</sub>O at 30°C.**

Water (ml)	C <sub>60</sub> solution (ml)	Brij35 + C <sub>12</sub> E <sub>12</sub> O- Propanol (ml)	Solution
1.0	0.1	0.51	Clear
1.0	0.2	0.79	Clear
1.0	0.3	1.43	Clear
1.0	0.4	1.81	Clear
1.0	0.5	2.2	Clear
1.0	0.6	2.57	Clear
1.0	0.7	2.66	Turbid
1.0	0.8	2.98	Clear

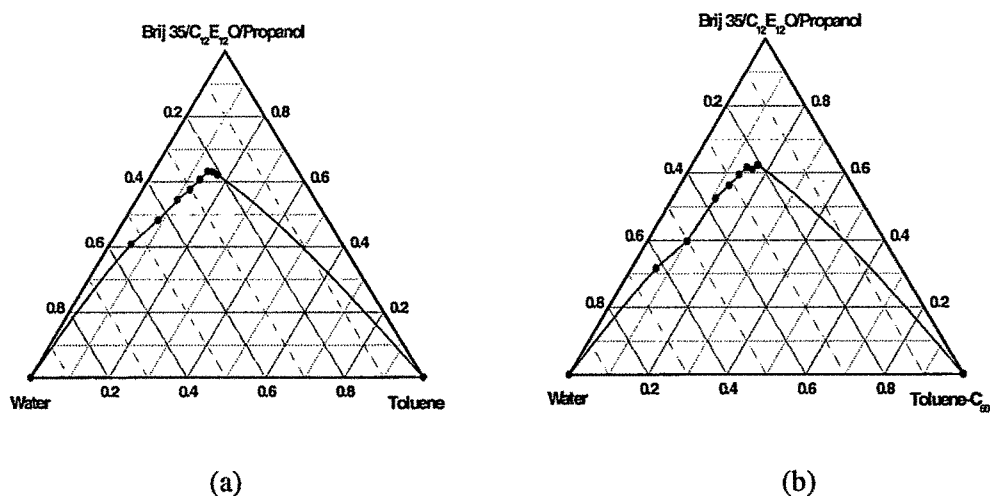


**Figure 3.18** Triangular phase diagram for  $C_{12}E_{12}O$  + Brij 35 (1:1) in (a) absence and (b) presence of [60]fullerene.

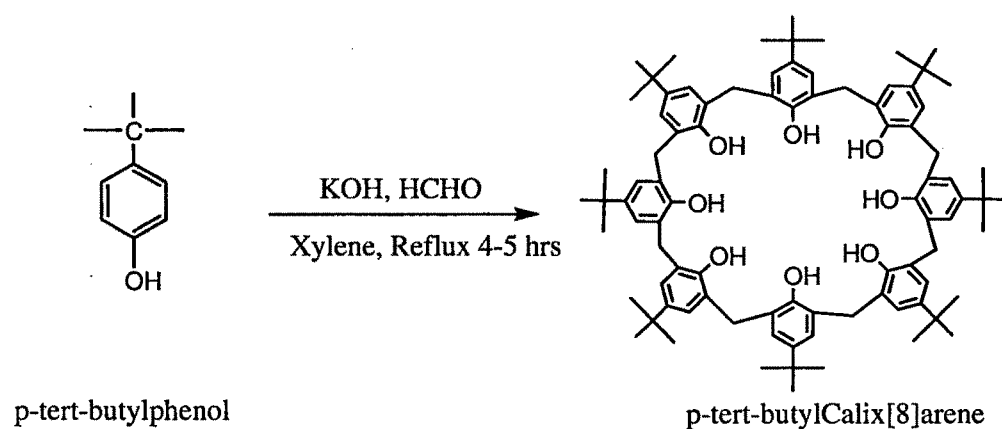
The results of the microemulsion studies are summarized in Table 3.14. It can be seen that the linear surfactant Brij 35 forms a better microemulsion with the  $C_{60}$  than Span 60. Comparing the structural features of these two surfactants, the Brij 35 is a linear surfactant with a small head group that is compatible with the nonaqueous solvent whereas the Span 60 surfactant has a head that is big and is a ring structure. These structural differences seem to influence the formation of the microemulsions.

**Table 3.14.** Summary of the monophasic and biphasic regions formed by the system of C<sub>60</sub>-Toluene-Water and surfactants at different temperatures.

Surfactant	Temperature (°C)	without C <sub>60</sub>			with C <sub>60</sub>		
		Total area (cm <sup>2</sup> )	Biphasic (cm <sup>2</sup> )	Monophasic (cm <sup>2</sup> )	Total area (cm <sup>2</sup> )	Biphasic (cm <sup>2</sup> )	Monophasic (cm <sup>2</sup> )
Span 60	30°C	13.2	10.8	2.4 (18.2%)	13.4	10.3	3.1 (23.1%)
	40°C				14.8	11.5	3.3 (22.3%)
	50°C				13.4	9.8	3.6 (26.9%)
Brij 35	30°C	12.5	9.1	3.4 (27.2 %)	12.7	8.5	4.2 (33.1%)
	40°C				12.6	8.2	4.4 (34.9%)
Brij 98	30°C	12.9	8.3	4.6 (35.6 %)	13.7	8.9	4.8 (35.0%)
C <sub>12</sub> E <sub>12</sub> O	30°C	12.6	9.5	3.1 (24.6 %)	13.4	9.1	4.3 (32.1%)
Brij 35+ C <sub>12</sub> E <sub>12</sub> O (1:1)	30°C	12.2	8.8	3.4 (27.9%)	12.7	8.5	4.2 (33.7%)

### 3.3. CALIX[8]ARENE AS SUPRAMOLECULAR HOST MOLECULE FOR [60]FULLERENE

Calixarenes are basket-shaped molecules and of potential interest for host-guest complexation studies. In view of our interest in the water-solubilization studies of [60]fullerene, calix[8]arene was selected as a suitable host molecule for the encapsulation of the [60]fullerene. Calix[8]arene has been synthesized in a number of ways and has been extensively reported in literature. However here we have used the “one-step” procedure, which involves the base catalyzed reaction of p-substituted phenol (p-tert-butyl phenol) and paraformaldehyde as reported [83] and the pure p-tert-butyl calix[8]arene was isolated using the same method mentioned. This reaction is shown in Scheme 3.1.



**Scheme 3.1** Synthesis of base catalyzed p-tert-butyl calix[8]arene

This base catalyzed reaction is carried out under the basic conditions using KOH as a base and paraformaldehyde in refluxing xylene, the cyclic octamer is isolated in a good yield. All the reactions were carried out in a well-ventilated hood. Initially the reaction assembly was purged with nitrogen before addition of the reactants. After addition of the reactants the contents were allowed to reflux. After 30-45 minutes, the reaction mixture becomes homogeneous and as the reflux starts water was separated from the reaction mixture and that was collected in the Dean-Stark apparatus. After 1-1.5 hrs a white

precipitate starts to form. Completion of reaction was conformed by TLC. Precipitates formed were collected by filtration and dried. These precipitates were dissolved in boiling chloroform for recrystallization. The yield was 62.7 % and the product obtained was characterized by FTIR,  $^1\text{H}$ -NMR,  $^{13}\text{C}$ -NMR, LC- mass spectroscopy.

The FTIR spectrum is shown in Figure 3.19. The major bands in FTIR-spectrum are at  $3220.55\text{cm}^{-1}$  (-OH stretching (ArOH)),  $2956.31\text{ cm}^{-1}$ (C-H stretching),  $1487.30\text{ cm}^{-1}$ (C-H bending),  $1603.22\text{ cm}^{-1}$ (C=C stretching) (aromatic conjugation),  $1392.56\text{ cm}^{-1}$ (C-H deformation ( $(\text{CH}_3)_3\text{-C-}$ )),  $1205.11, 1248.51\text{ cm}^{-1}$  (skeletal  $(\text{CH}_3)_3\text{-C-}$ ),  $1116.68\text{ cm}^{-1}$ (C-O stretching),  $874.99\text{ cm}^{-1}$  (-C-H out-of-plane deformation) (1 hydrogen atom).

The  $^1\text{H}$ -NMR of the p-tert-butyl calix[8]arene is shown in Figure 3.20 which shows a distinct separation of the proton signals. The signal assigned to the protons attached to aromatic carbons are  $\delta$  9.6(s,1H,ArOH), 7.20(m,3H,ArH), to aliphatic carbons are 3.5(s,2H, $\text{CH}_2$ ), 1.2(s,9H, $\text{C}(\text{CH}_3)_3$ ).  $^{13}\text{C}$ MR spectrum is shown in Figure 3.21. The signals obtained for the aliphatic carbons are  $\delta$  32.45 ppm (s, $\text{C}(\text{CH}_3)_3$ ), 25.07 ppm (q, $\text{C}(\text{CH}_3)_3$ ), to aromatic carbons are 25.73 ppm (t, $\text{ArCH}_2\text{Ar}$ ), 144.83 ppm (s,C-OH), 146.73, 128.83, 125.64 ppm (aromatic carbon).

A LC- MS mass spectrum is shown in the Figure 3.22, which shows the sharp peak at 1297 which is same as the calculated molecular weight of the p-tert-butyl calix[8]arene. All the results obtained were matching with those reported in literature.

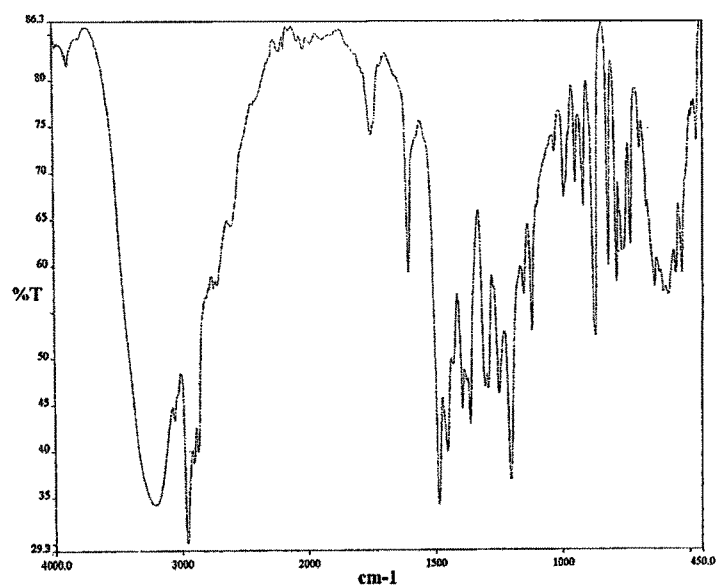


Figure 3.19. FTIR-Spectra of p-tert-butyl calix[8]arene.

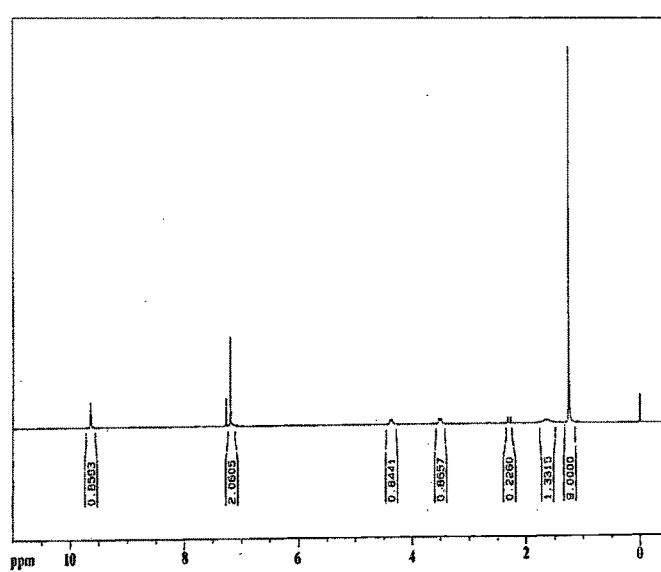


Figure 3.20. <sup>1</sup>H-NMR Spectra of the p-tert-butyl calix[8]arene

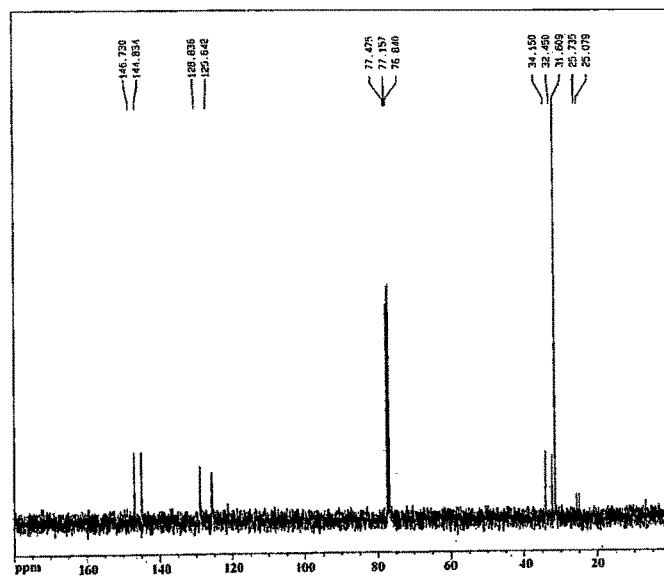


Figure 3.21  $^{13}\text{C}$ -NMR spectra of p-tert-butyl calix[8]arene

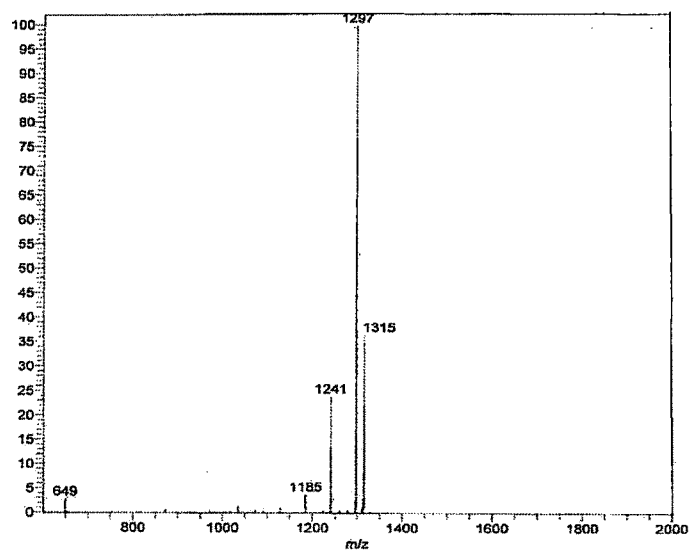
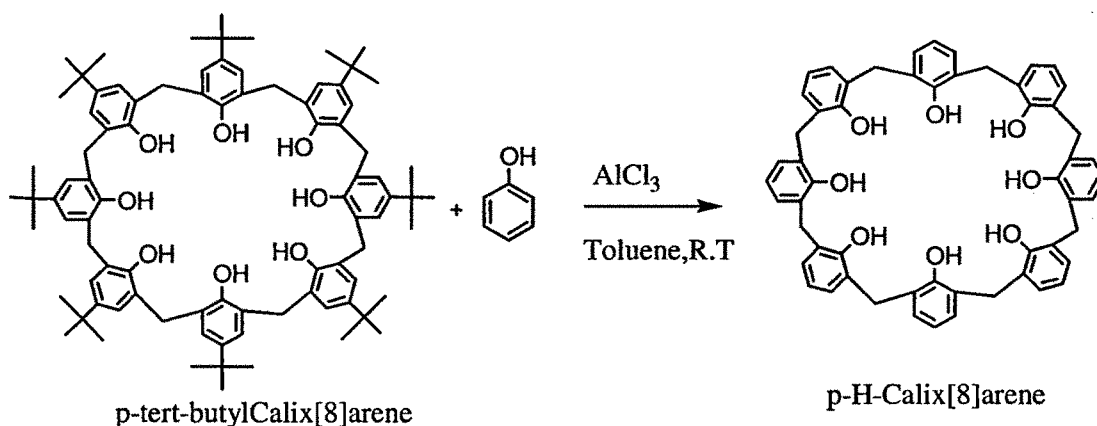


Figure 3.22. Mass spectra of the p-tert-butyl calix[8]arene.



Above all data confirmed the formation of p-tert-butyl calix[8]arene. Since the main aim of this work is to prepare water-soluble host molecule for [60]fullerene, so in addition to this from the synthesized p-tert-butyl calix[8]arene tert-butyl group was removed by a reverse Friedel-Crafts reaction involving treatment of the tert-butylcalix[8]arene with an excess of  $\text{AlCl}_3$  in the presence of an acceptor such as phenol.

In the reaction procedure after mixing reactants in the proper proportion a heterogeneous mixture was formed and to that anhydrous  $\text{AlCl}_3$  was added at once and mixture was continued to stirrer, which rapidly turned red within in 15 minutes. This becomes dark as time progresses. A viscous deep red sticky phase was separated on the walls of the flask. This is a room temperature reaction and was monitored by TLC and continued for 3 hrs. After completion of the reaction, the reaction mixture was poured in to ice-HCl mixture and organic phase was separated and was neutralized using water. After that solvent from the organic phase was removed using rotary evaporator under pressure which gives orange solid with 64.5% yield. The product was recrystallised from methanol/chloroform to obtained light gray solid. The reaction is shown in Scheme 3.2.



**Scheme 3.2** Synthesis of p-H-Calix[8]arene by Reverse alkylation process

The dealkylated product obtained was characterized through FTIR and  $^1\text{H}$  NMR-spectroscopy.

The major bands in the FTIR spectrum show that the peaks are at  $3212.71\text{cm}^{-1}$  (-OH stretching (ArOH)),  $2957.95\text{ cm}^{-1}$  (C-H stretching),  $1486.89\text{ cm}^{-1}$  (C-H bending),  $1602.17\text{ cm}^{-1}$  (C=C Stretching) (Aromatic conjugation),  $1117.61\text{ cm}^{-1}$  (C-O stretching),  $868.33\text{ cm}^{-1}$  (-C-H Out-of- plane deformation) (1 H atom). The FTIR Spectra is shown in Figure 3.23 from which we can clearly see the disappearance of the peak at  $1392.56\text{ cm}^{-1}$  which gives the conformation that the tert-butyl group was totally removed.

The  $^1\text{H}$  NMR is shown in Figure 3.24. The signals assigned to the protons are  $\delta$  9.34(s, 1H, ArOH), 7.20(m, 2H, ArH), 6.85(s, 1H, ArH), 4.23(s, 2H, CH<sub>2</sub>). There is no peak at 1.2 ppm that clearly indicated the removal of the tert-butyl group from the upper rim of the p-tert-butyl calix[8]arene.

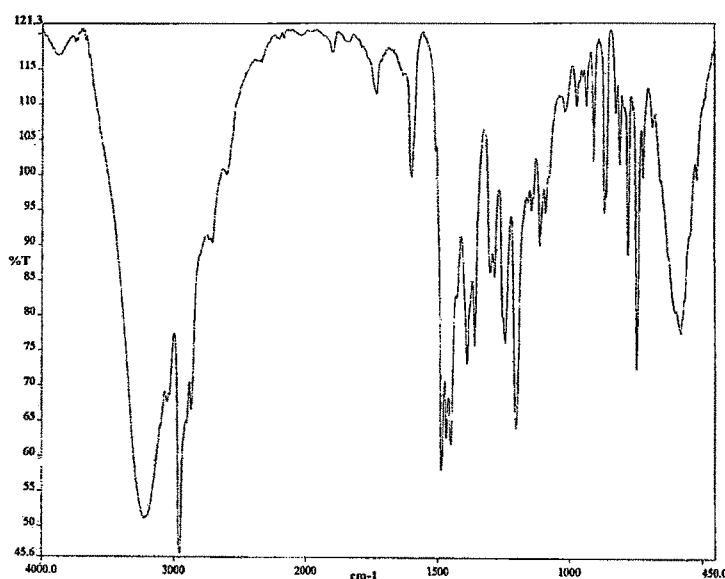


**Figure 3.23.** FTIR-spectra of p-H calix[8]arene

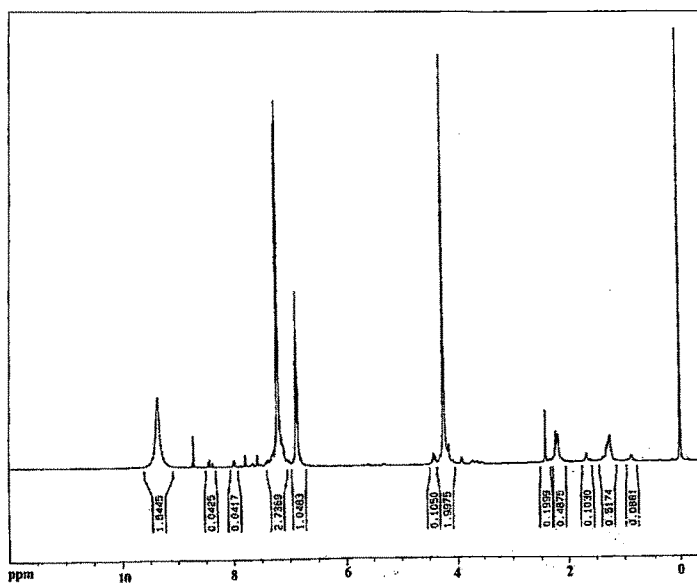
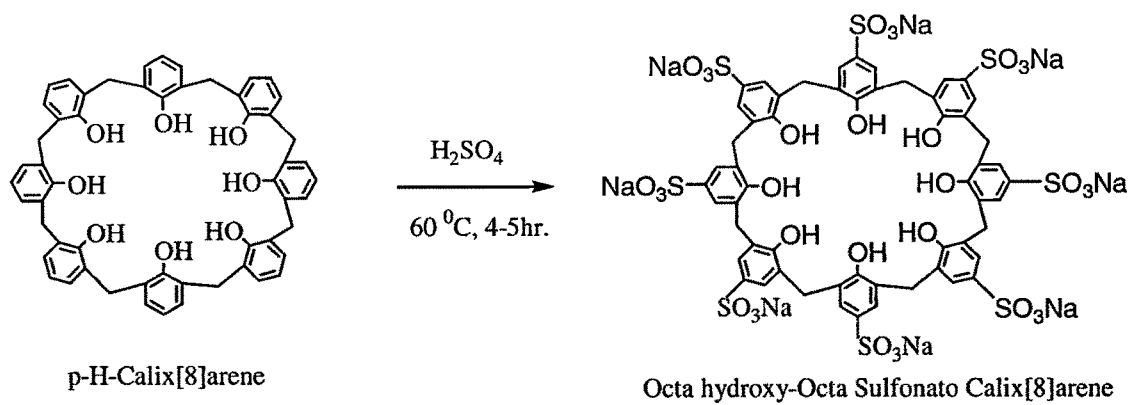
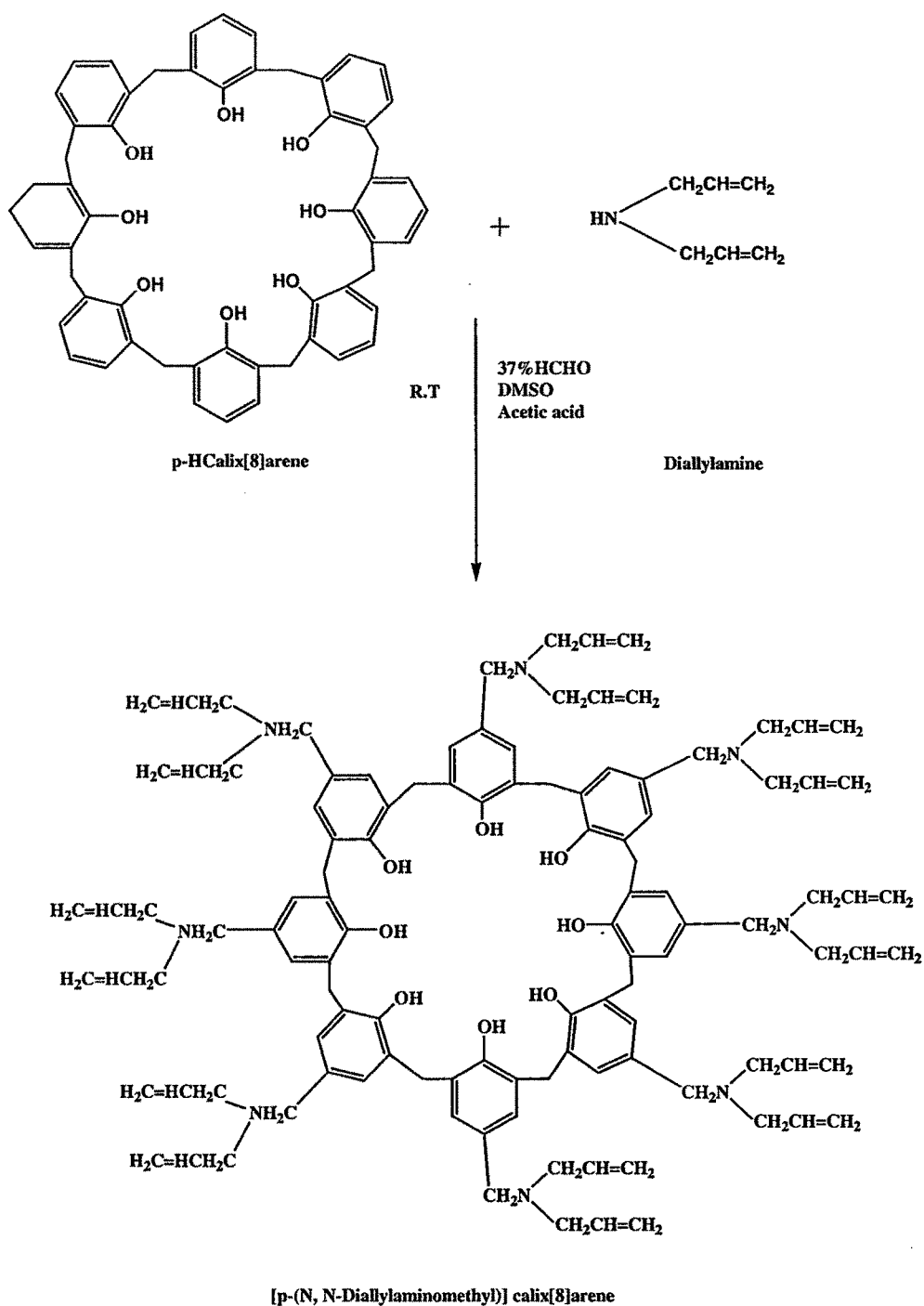


**Figure 3.24.**  $^1\text{H}$ -NMR spectra of p-H calix[8]arene

The unsubstituted p-H-calix[8]arene synthesized as mentioned above was further used to synthesize the water-soluble p-sulfonatedcalix[8]arene and[p-(N,N-diallyl aminomethyl)] calix[8]arene. The  $-\text{SO}_3\text{H}$  group was introduced at the upper rim of the calix[8]arene by sulfonation with concentrated  $\text{H}_2\text{SO}_4$  with 55.5% yield. The diallyl group was introduced by using diallylamine with 51% yield. Both the functionalized calix[8]arene molecules are highly water-soluble solid with greyish white and light yellow colour and were characterized through FTIR,  $^1\text{H}$ -NMR,  $^{13}\text{C}$ -NMR spectroscopy. The reactions are given in Scheme 3.3 for the sulphonyl group introduction and in Scheme 3.4 for the diallylamine group introduction respectively.



**Scheme 3.3.** Synthesis of p-Sulfonato calix[8]arene



**Scheme 3.4.** Synthesis of [p-(N, N-Diallylaminomethyl)]calix[8]arene

The major bands in FT-IR spectrum of p-sulfonatedcalix[8]arene shows peaks at 3455  $\text{cm}^{-1}$  (-OH stretching), 2915  $\text{cm}^{-1}$  (C-H stretching), 1450  $\text{cm}^{-1}$  (-CH<sub>2</sub>), 1142  $\text{cm}^{-1}$  (SO<sub>3</sub><sup>-</sup> symmetric), 863.3  $\text{cm}^{-1}$  (-C-H out-of- plane deformation)(1H atom). The FT-IR spectrum is shown in Figure 3.25.

The major bands in FT-IR spectrum of [p-(N, N-Diallylaminomethyl)]calix[8]arene shows peaks at 3265.59  $\text{cm}^{-1}$  (-OH stretching (ArOH)), 2976.26  $\text{cm}^{-1}$  (C-H stretching), 1480.52  $\text{cm}^{-1}$  (C-H bending), 1589.40  $\text{cm}^{-1}$  (C=C stretching)(aromatic conjugation), 1107.18  $\text{cm}^{-1}$  (C-O stretching), 1155.40, 1139.97  $\text{cm}^{-1}$  (C-N stretching), 879.57  $\text{cm}^{-1}$  (-C-H out-of- plane deformation)(1H atom), =C-H stretching and deformation: 3074.63  $\text{cm}^{-1}$  (CH<sub>2</sub> stretching), 993.37  $\text{cm}^{-1}$  (CH out-of-plane deformation), 916.22  $\text{cm}^{-1}$  (CH<sub>2</sub> out-of-plane deformation), 1415.80  $\text{cm}^{-1}$  (CH<sub>2</sub> in-plane deformation), 1614  $\text{cm}^{-1}$  (C=C stretching)(nonconjugated). The FT-IR Spectrum for p-(N, N-Diallylaminomethyl)]calix[8]arene is shown in Figure 3.26.

The <sup>1</sup>H-NMR of p-sulfonated calix[8]arene is shown in the Figure 3.27. The two signals were obtained at  $\delta$  7.80 ppm (m, 2H, ArH), 3.86 ppm (s, 2H, CH<sub>2</sub>).

The PMR spectrum of [p-(N, N-Diallylaminomethyl)]calix[8]arene is shown in Figure 3.28.

The signal assigned to the protons attached to aromatic carbon are  $\delta$  9.46 ppm (s, 1H, OH), 7.26 ppm (s, 2H, ArH), 4.31 ppm (d, 2H, Ar-CH<sub>2</sub>-Ar), 3.44 ppm (s, 2H, ArCH<sub>2</sub>N), to aliphatic carbons are 5.86 ppm (m, 2H, C-CH=C-), 5.19 ppm (m, 4H, C=CH<sub>2</sub>), 3.00 ppm (d, 4H, NCH<sub>2</sub>C).

The <sup>13</sup>C-NMR spectrum of the [p-(N, N-Diallylaminomethyl)]calix[8]arene is shown in the Figure 3.29. The peaks related to aromatic carbons are to aliphatic carbon are  $\delta$  29.69 ppm (s, N-CH<sub>2</sub>), 31.68 ppm (s, CH<sub>2</sub>-N), 56.10 ppm (d, CH<sub>2</sub> attached to CH=CH<sub>2</sub>), 56.82 ppm (t, CH attached to CH=CH<sub>2</sub>), to aromatic carbons are 135.84 ppm (s, C-OH), 117.31 ppm, 129.04 ppm (s, -CH<sub>2</sub> aromatic carbons).

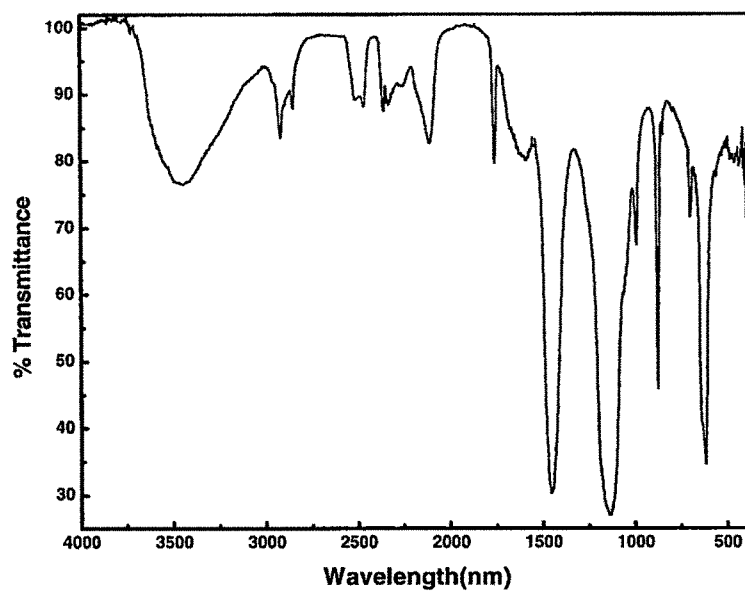


**Figure 3.25.** FTIR spectrum of p-sulfonatocalix[8]arene

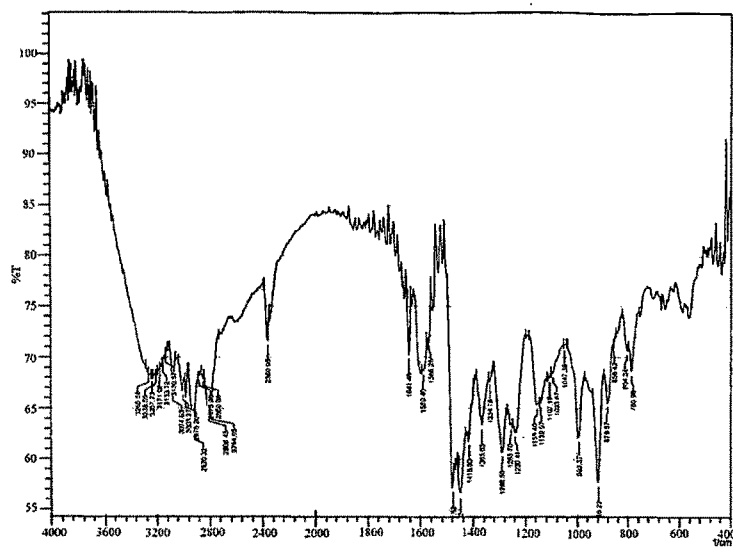


**Figure 3.26.** FTIR Spectra of [p-(N, N-Diallylaminomethyl)]calix[8]arene.

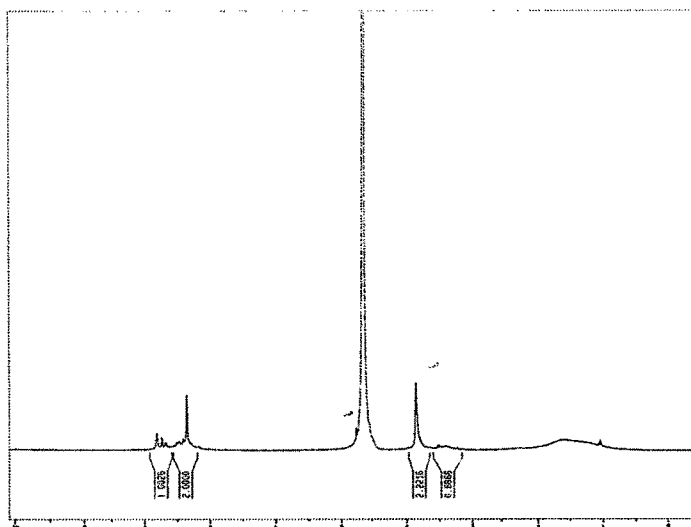


Figure 3.27.  $^1\text{H}$ -NMR spectra of p-sulfonatocalix[8]arene

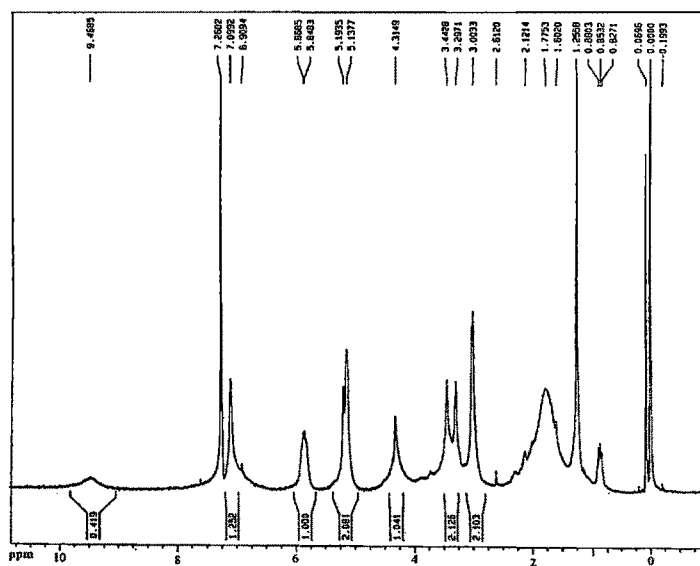
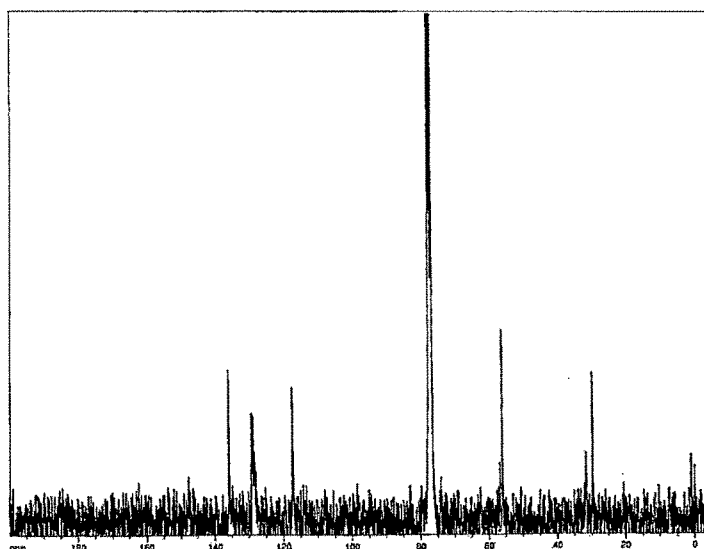


Figure 3.28.  $^1\text{H}$  NMR spectra of [p-(N, N-Diallylaminomethyl)]calix[8]arene.





**Figure 3.29.**  $^{13}\text{C}$ -NMR spectra of [p-(N, N-diallylaminomethyl)]calix[8]arene

Since calixarenes have a cavity composed of benzene rings (which behaves like  $\pi$ -donors) while fullerenes are  $\pi$ -systems with good electron affinity, these two can form inclusion complex through  $\pi$ -  $\pi$  interaction. Keeping this in view the synthesis of p-sulfonated calix[8]arene-[60]fullerene and [p-(N,N-Diallylaminomethyl)]calix[8]arene-[60]fullerene inclusion complex were achieved in a mixed organic solvent system containing DMF and toluene where both p-sulfonato calix[8]arene and [p-(N, N-Diallylaminomethyl)]calix[8]arene formed a homogeneous reaction medium with [60]fullerene.

Initially the colour of the reaction mixture of p-sulfonated calix[8]arene-[60]fullerene was violet and it was observed that the colour did not remain as such and changed to brown colour with passage of time. This indicates that there was some interaction between p-sulfonated calix[8]arene and [60]fullerene. This was a room temperature reaction and reaction was continued for a week. After that solvent from the reaction mixture was removed through rotary evaporator giving buff colour solid which is highly water-soluble and formed a yellow colored solution.

The confirmation of the formation of the inclusion complex between the water soluble p-sulfonatocalix[8]arene and [60]fullerene was obtained from UV-VIS absorbance spectroscopy. The [60]fullerene shows an absorbance maxima at around 330 nm in toluene [Figure 3.2a] which is water-insoluble, whereas p-sulfonatocalix[8]arene shows a very weak and broad absorbance at around 266 nm in water [Figure 3.30]. However the spectrum of the p-sulfonatocalix[8]arene-[60]fullerene complex in water showed a sharp and intense absorbance peak at 220nm. Though [60]fullerene is insoluble in water, it is soluble in organic solvents like toluene, benzene and other hydrocarbon solvents and shows strong absorbance at ~260nm. Thus the presence of a strong absorbance at 266 in water can be assigned to the [60]fullerene that is encapsulated into the apolar cavity of p-sulfonatocalix[8]arene.

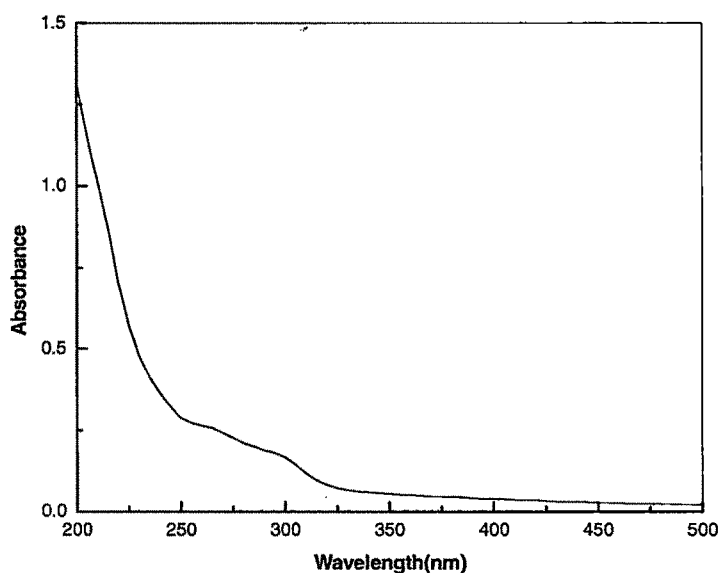


**Figure 3.30.** UV-Visible spectra of p-sulfonatocalix[8]arene in water.

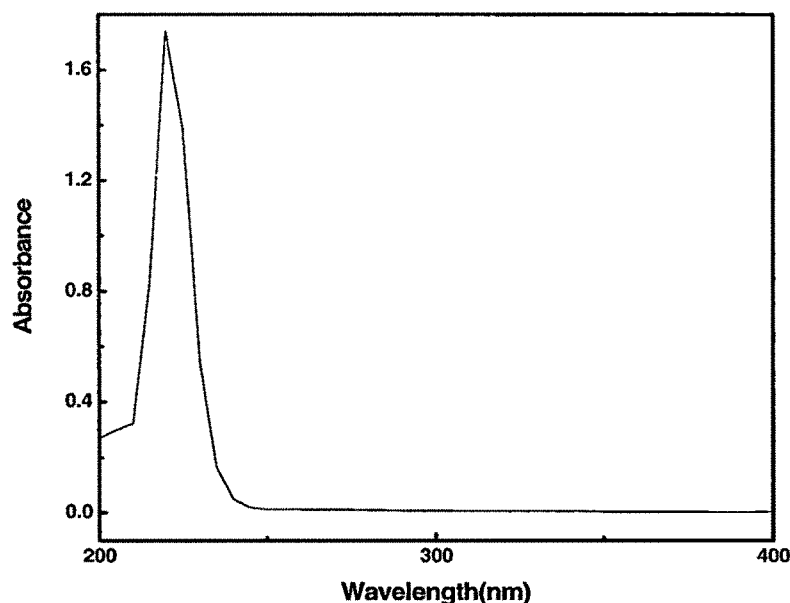


**Figure 3.31.** UV-visible spectra of p-sulfonatocalix[8]arene-[60]fullerene complex in water.

The nature of the interaction between [60]fullerene and the water-soluble p-sulfonatocalix[8]arene is an important feature of this study. The UV-VIS absorbance studies do not give any indication about the nature of the binding between [60]fullerene and p-sulfonatocalix[8]arene.

To understand the nature of the interaction between the two an aqueous solution of the complex was shaken with toluene for few minutes and the UV absorbances of the aqueous phase [Figure 3.32] was recorded. The aqueous phase showed the typical absorbance of [60]fullerene with the slight absorbance peak corresponding to that p-sulfonatocalix[8]arene. The organic phase study shows the absence of both host and guest molecule in the toluene layer. This suggests that there is no covalent bond formation between the two.

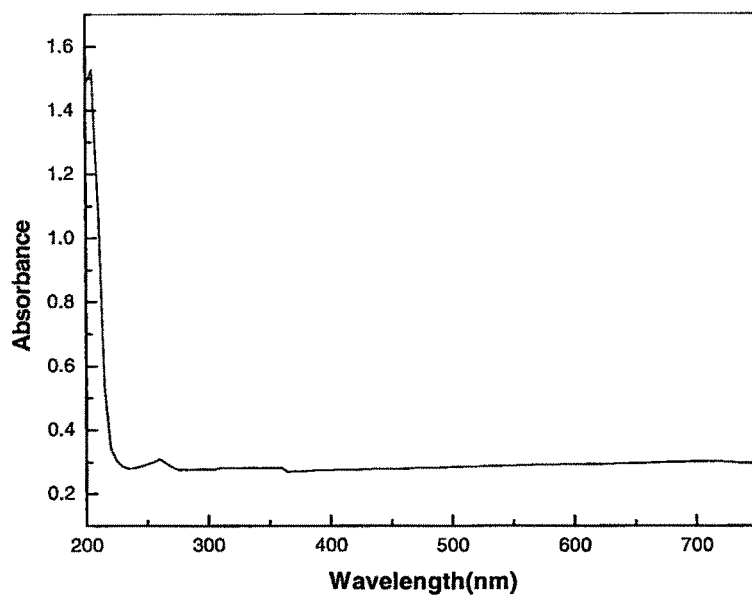


**Figure 3.32** UV-Visible spectra of p-sulfonatocalix[8]arene-[60]fullerene complex in aqueous layer.

Further conformation of this synthesized supramolecular complex of p-sulfonatocalix[8]arene-[60]fullerene was found by taking its FTIR spectra. The major bands obtained are at  $3452\text{ cm}^{-1}$  (-OH stretching),  $1426\text{ cm}^{-1}$  (-C-C in  $\text{C}_{60}$ ),  $1141\text{ cm}^{-1}$  ( $\text{SO}_3^-$  symmetric). The FT-IR spectra is shown in Figure 3.34.

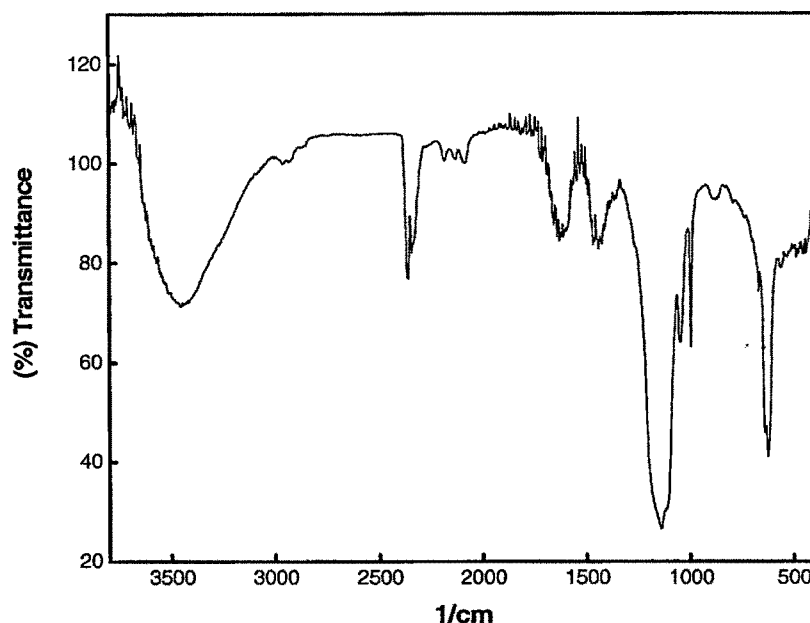


**Figure 3.33.** FTIR-spectra of p-sulfonatocalix[8]arene-[60]fullerene complex.

Similarly the reaction between p-N, N diallylaminomethyl calix[8]arene and [60]fullerene was carried out following the same mixed solvent procedure as used for the p-sulfonatocalix[8]arene-[60]fullerene complex. The reaction was continued for one week when the color of the reaction mixture changed from violet to reddish brown. From the colour change it was confirmed that there was some interaction between the [60]fullerene and the diallylaminomethyl calix[8]arene. The interaction between p-N,N Diallylaminomethyl calix[8]arene and [60]fullerene was studied on the basis of the UV absorbance spectra of the complex in the aqueous phase and the organic phase. The water soluble complex shows a absorbance at 288nm and at 340nm. The UV-VIS spectrum is shown in Figure 3.35.

The UV-absorbance spectra of the aqueous phase of the water-soluble complex shows a typical peak at 262 nm disappearing the peak of [60]fullerene. Study of the organic layer of the water-soluble complex shows sharp peak at 335nm which corresponds to a [60]fullerene absorbance. This study indicates that the covalent bond was formed between these two molecules and was not stable in the organic phase and we can easily

observe it from the UV-visible spectra which are taken after mixing aqueous solution of the complex in organic solvent. In the toluene layer may be the bond which is form between [60]fullerene and p-N,N Diallylaminomethyl calix[8]arene by the sharing of electrons was broken and again we are getting a sharp absorbance peak corresponding to [60]fullerene in the organic layer.

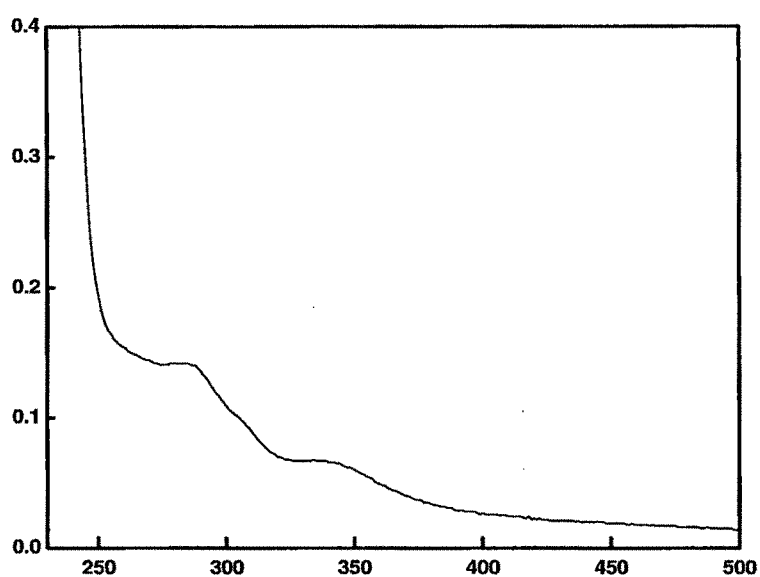


**Figure 3.34.** UV-Visible spectra of [p-(N, N-Diallylaminomethyl)]calix[8]arene-[60]fullerene complex.

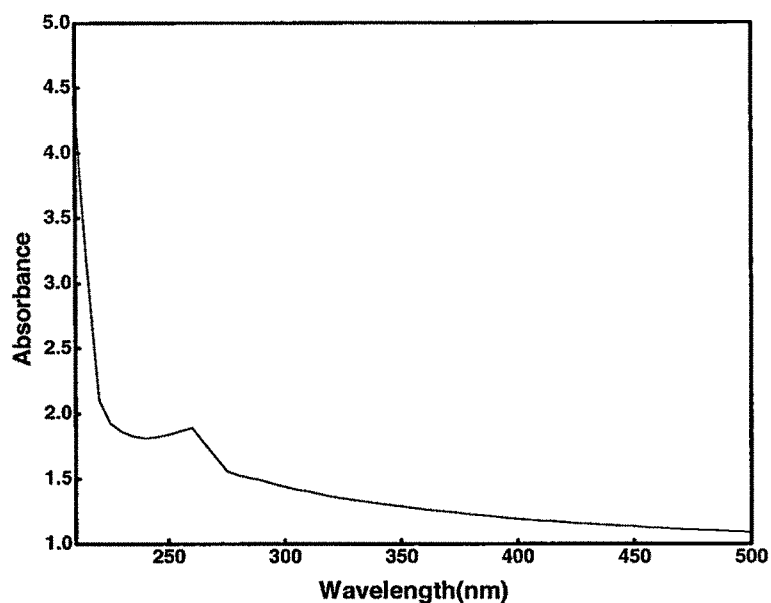


**Figure 3.35.** UV-Visible spectra of [p-(N, N-Diallylaminomethyl)]calix[8]arene-[60]fullerene complex in aqueous layer.

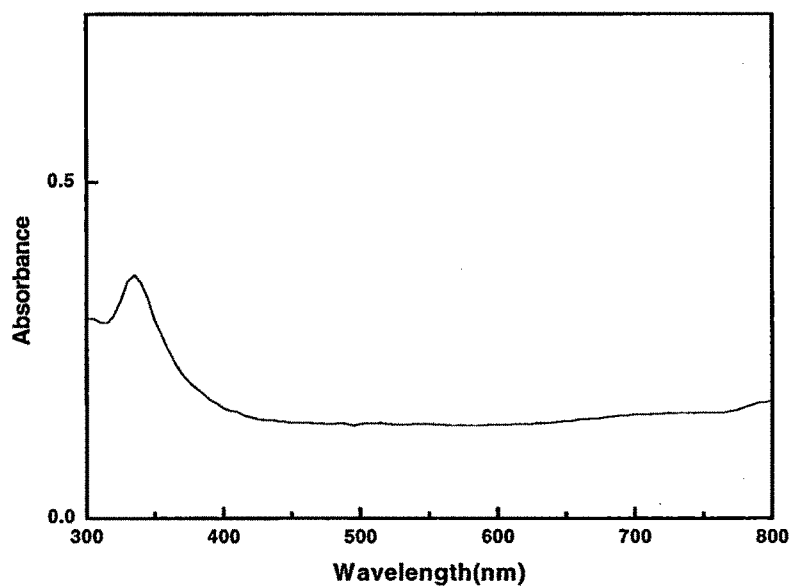


**Figure 3.36** UV-Visible spectra of [p-(N, N-Diallylaminomethyl)]calix[8]arene-[60]fullerene complex in toluene layer.

### 3.4. CYCLODEXTRINS AS SUPRAMOLECULAR HOST MOLECULES FOR [60]FULLERENE

One of the potential applications of [60]fullerene is in biomedical applications. Apart from its radical scavenging properties it has been reported that it shows ferromagnetic behavior [114]. It has been reported that [60]fullerene shows ferromagnetism in pristine state when exposed to ultraviolet radiation over a period of time. This has potential for application as MRI contrast agent. However the major drawback of this molecule is its (1) aqueous solubility and (2) biocompatibility. Pristine fullerene is water-insoluble and so has to be made water-soluble for further applications. [60]fullerene was made water-soluble by encapsulating it in a water-soluble molecule like  $\gamma$ ,  $\beta$ -cyclodextrin molecule by using solvent free synthesis method. The synthesized water-soluble complexes were characterized through FTIR, UV spectroscopy. The inclusion complex was also characterized by thermogravimetric analysis.

The major bands in FT-IR spectrum of  $\gamma$ -cyclodextrin-[60]fullerene complex show peak at  $3343.4\text{ cm}^{-1}$  (O-H Stretching),  $2924.03\text{ cm}^{-1}$  (C-H Stretching),  $1415.2\text{ cm}^{-1}$  ( $\text{C}_{60}$ ),  $1028\text{ cm}^{-1}$  (C-C Stretching), is shown in the figure 3.38.

In case of  $\beta$ -cyclodextrin-[60]fullerene complex the peaks obtained in FT-IR spectrum are at  $3358.29\text{ cm}^{-1}$  (O-H Stretching),  $2924.03\text{ cm}^{-1}$  (C-H Stretching),  $1182, 577\text{ cm}^{-1}$  ( $\text{C}_{60}$ ),  $1028.18\text{ cm}^{-1}$  (C-C Stretching) is shown in Figure 3.39.

The UV-visible spectra also confirms the complex formation of  $\gamma$ ,  $\beta$ -cyclodextrin molecule with [60]fullerene and the UV- Spectra of  $\gamma$ -cyclodextrin-[60]fullerene complex is shown in Figure3.40 In which we can easily see the slight absorbance corresponding to [60]fullerene at 324nm. UV- Spectra of  $\beta$ -cyclodextrin-[60]fullerene complex shown in Figure 3.41.



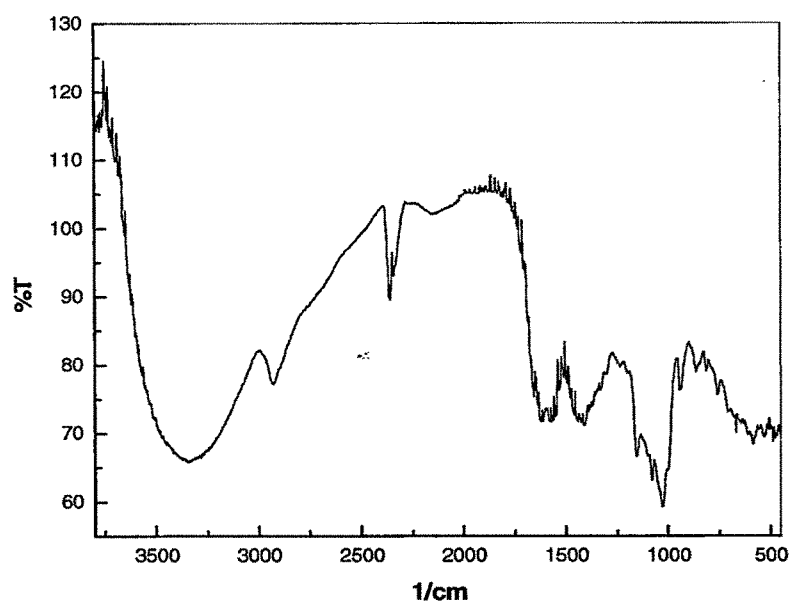


**Figure 3.37.** FTIR Spectra of  $\gamma$ -cyclodextrin-[60]fullerene complex.

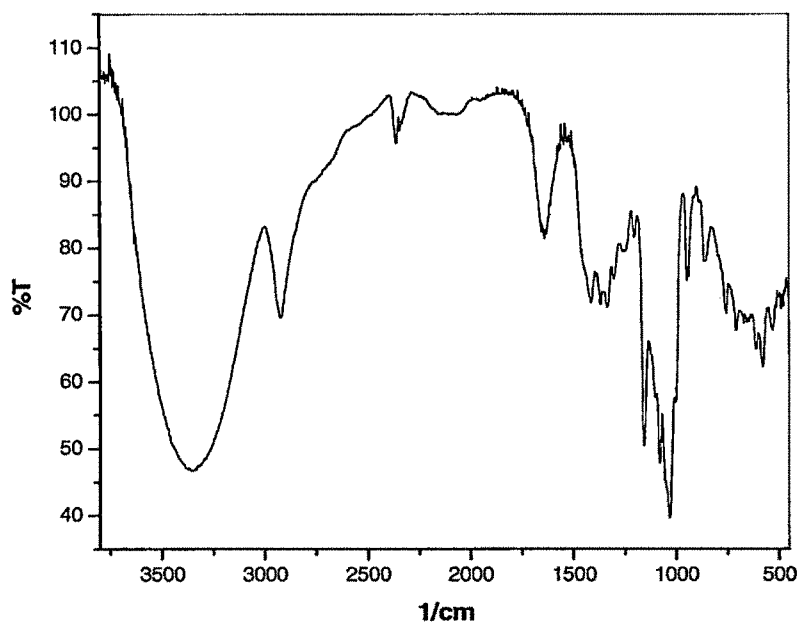


**Figure 3.38.** FTIR Spectra of  $\beta$ -cyclodextrin-[60]fullerene complex.

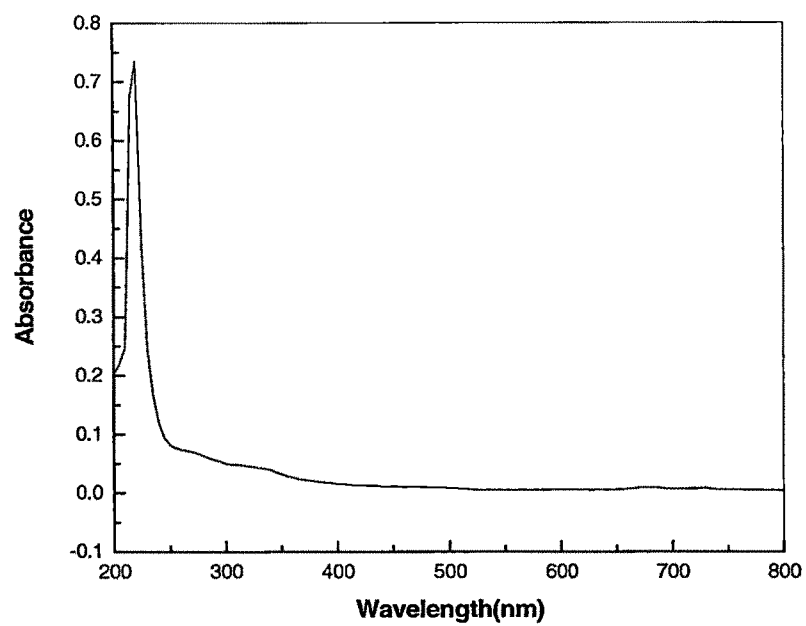


**Figure 3.39.** UV- Spectra of  $\gamma$ -cyclodextrin-[60]fullerene complex.

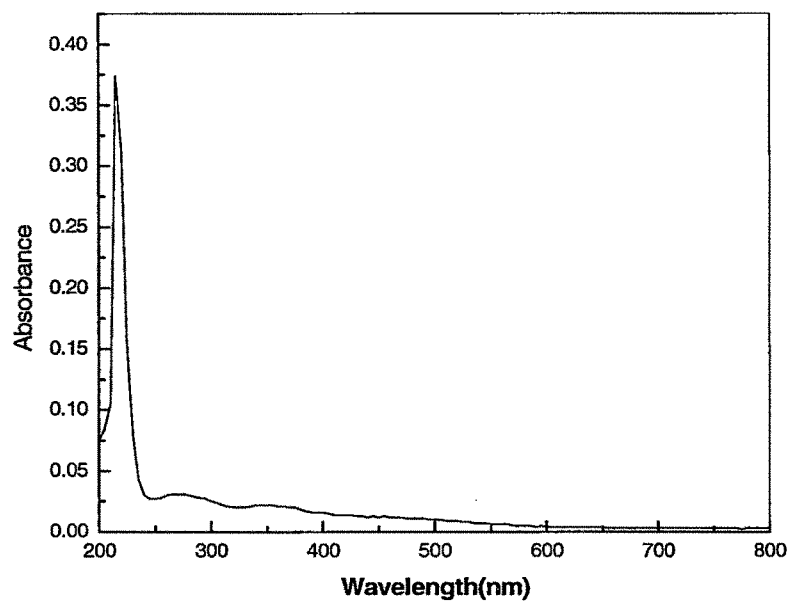


**Figure 3.40.** UV- Spectra of  $\beta$ -cyclodextrin-[60]fullerene complex

TGA analysis of the product showed that the [60]fullerene-  $\gamma$ -cyclodextrin adduct were in the stoichiometric ratio of 1:2. i.e. each fullerene molecule was encapsulated by two cyclodextrin molecules. The thermogram is shown in the Figure 3.42.

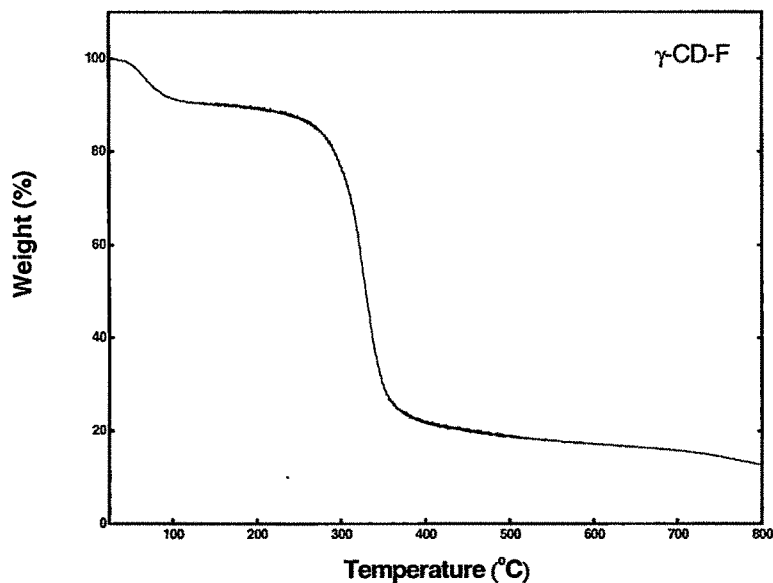


**Figure 3.41.** Thermogram of  $\gamma$ -cyclodextrin-[60]fullerene complex

We have irradiated  $\gamma$ -cyclodextrin capped fullerene ( $C_{60}$ ) with ultraviolet radiation under different conditions and studied the effect on magnetic property of fullerene. Magnetic measurements were made on a SQUID magnetometer. The magnetisation vs field plot is shown in Figure 3.43.

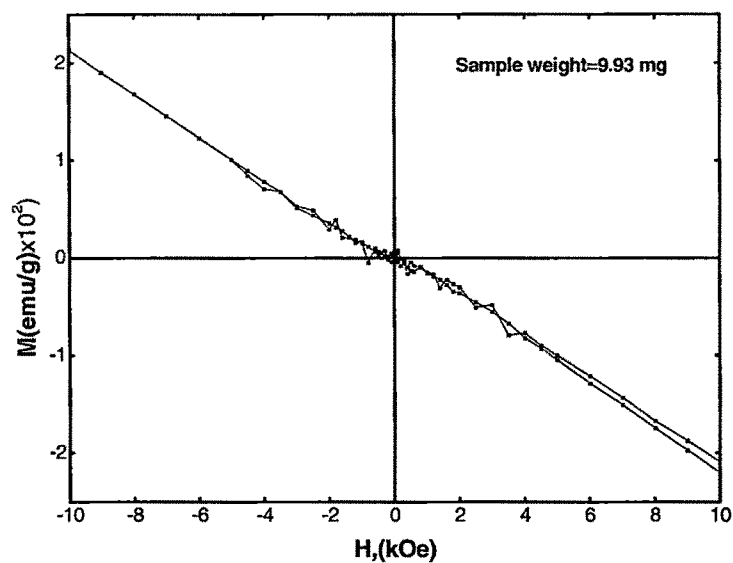


**Figure 3.42.** Magnetisation of the capped  $C_{60}$  as a function of DC magnetic field.

Though the sample did not show any ferromagnetic behaviour but at low fields there seems to be an odd response to the magnetic field. This is shown in the Figure 3.44.

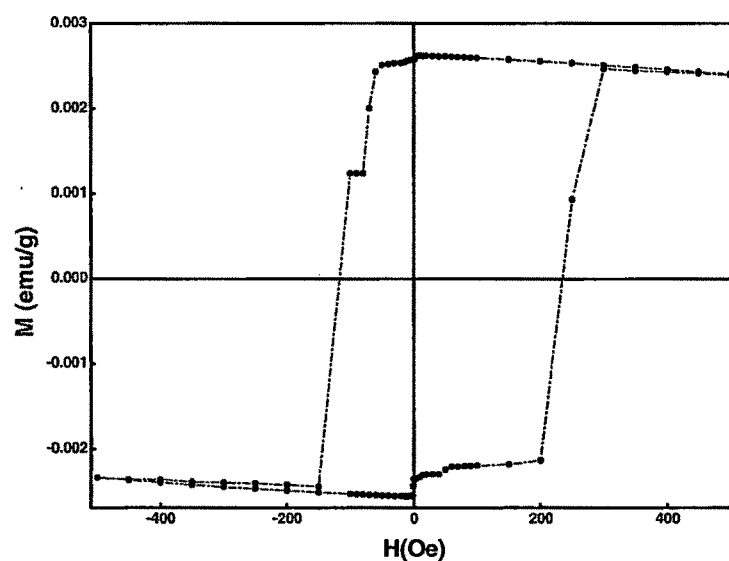


**Figure 3.43** The typical magnetization as a function of the dc magnetic field for the sample irradiated for 24h.

The capping molecule i.e. cyclodextrin is transparent to the UV radiation as has been found from solution studies, unlike the  $C_{60}$  molecule that is known to strongly absorb in the ultraviolet region of the spectrum in a toluene solution. Future studies would include the effect of ultraviolet treatment on the complex in terms of the water-solubility and solution absorption in the ultraviolet region. Even though the capping was there and the overall response being diamagnetic, there seems to be some component of ferromagnetism. The nature of this component and its origin needs to be investigated more thoroughly. The irradiated samples were analysed by FTIR and UV-VIS spectroscopy. There is no apparent change in the structure of the [60]fullerene molecule before and after irradiation. The spectra are shown in Figure 3.45 and Figure 3.46.

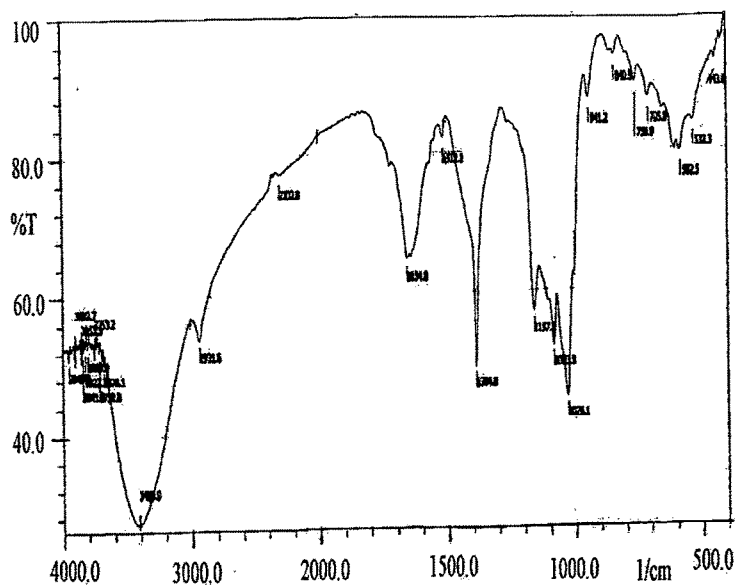


**Figure 3.44.** FT-IR Spectra of the  $\gamma$ -cyclodextrin-[60]fullerene complex irradiated for 24hrs.

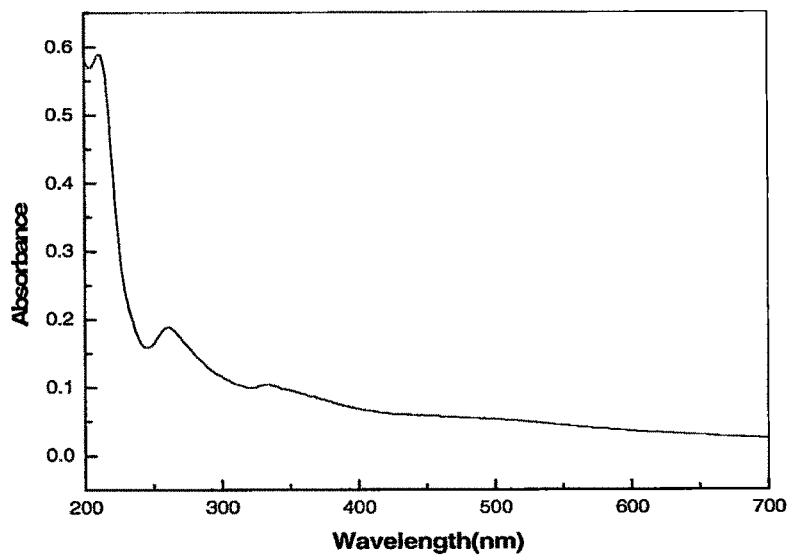


**Figure 3.45.** UV-Spectra of the  $\gamma$ -cyclodextrin-[60]fullerene complex irradiated for 24hrs.